Swiss J Geosci (2017) 110:811–831
DOI 10.1007/s00015-017-0279-y

Rocks control the chemical composition of surface water from the high Alpine Zermatt area (Swiss Alps)

Kurt Bucher[1] · **Wei Zhou**[1,2] · **Ingrid Stober**[3]

Received: 29 November 2016 / Accepted: 14 June 2017 / Published online: 30 June 2017

Abstract The study presents composition data of 87 surface water samples from high alpine catchments of the Zermatt area (Swiss Alps). The investigated area covers 170 km^2. It was found that the surface runoff acquires the dissolved solids mostly by reaction of precipitation water with the minerals of the bedrock. Total dissolved solids (TDS) vary from 6 to 268 mg L^{-1}. All collected water shows a clear chemical signature of the bedrock mineralogy. The contribution of atmospheric input is restricted to small amounts of ammonium nitrate and sodium chloride. NH_4 is a transient component and has not been detected in the runoff. Evaporation is not a significant mechanism for TDS increase in the Zermatt area. The chemical composition of the three main types of water can be related to the mineralogy of the dominant bedrock in the catchments. Specifically, Ca-HCO_3 (CC) waters develop from metamorphic mafic rocks and from carbonate-bearing schists. Mg-HCO_3 water originates from serpentinites and peridotites. Ca-SO_4 (CS) waters derive from continental basement rocks such as pyrite-rich granite and gneiss containing oligoclase or andesine. The collected data suggest that, together with reaction time, modal sulfide primarily controls and limits TDS of the waters by providing sulfuric acid for calcite (CC waters) and silicate (CS waters) dissolution. If calcite is present in the bedrock, its dissolution neutralizes the acid produced by sulphide weathering and buffers pH to near neutral to weakly alkaline conditions. If calcite is absent, the process produces low-pH waters in gneiss and granite catchments. The type of bedrock and its mineral assemblage can be recognized in water leaving very small catchments of some km^2 area. The large variety of water with a characteristic chemical signature is an impressive consequence of the richly diverse geology and the different rock inventory of the local catchments in the Zermatt area.

Keywords Surface water · Hydrogeochemistry · Zermatt Region · Water–rock interaction · Alpine catchments

1 Introduction

Dissolved solids and gasses in surface waters can derive from many different sources. Main contributions to the chemical composition of surface waters include atmospheric input, interaction with the biomass, discharge of mineralized groundwater, dissolution of minerals from soil and bedrock and anthropogenic input (Garrels and Mackenzie 1967; Raiswell 1984; Drever and Hurcomb 1986; Tranter et al. 1993; Brown et al. 1994; Aquilina et al. 1997; De Caritat and Saether 1997; Stober et al. 1999; Neal and Shand 2002). Separation of the different contributions is difficult in low-altitude catchments covered by vegetation (Hilberg and Riepler 2016).

Editorial handling: E. Gnos.

Electronic supplementary material The online version of this article (doi:10.1007/s00015-017-0279-y) contains supplementary material, which is available to authorized users.

✉ Kurt Bucher
bucher@uni-freiburg.de

[1] Institut für Geo- und Umweltnaturwissenschaften, Mineralogie-Petrologie, Albertstr. 23b, 79104 Freiburg, Germany

[2] Present Address: Swiss Gemmological Institute SSEF, Aeschengraben 26, 4051 Basel, Switzerland

[3] Karlsruhe Institute of Technology, Applied Geosciences, Adenauerring 20b, Bld. 50.40, 76131 Karlsruhe, Germany

In this study we investigated the composition of surface water in the high-altitude Zermatt area of the Swiss Alps characterized by thin or lacking biomass and soil cover. In these Alpine catchments the diverse potential contributions to the chemical composition of surface water are very limited (Pfeifer et al. 2000; Kilchmann et al. 2004). In bare-rock areas, the chemical weathering of rocks and minerals causes primarily solute acquisition of surface waters. These processes can be bio-mediated even in high-altitude catchments (Wadham et al. 2010). Chemical reaction of atmospheric precipitation with exposed fractured rocks is the main cause for the observed water composition. The catchments of the Zermatt area have extremely varied bedrock geology, including granite and gneiss, carbonate-bearing schists and marbles, mafic rocks derived from basalt and gabbro, and large bodies of olivine-bearing serpentinite. This diverse bedrock geology is reflected in the composition of water in streams, brooks and lakes of the Zermatt area.

Surface water–rock interaction in granitic or basaltic catchments at low altitude with vegetation cover has been the subject of many studies (e.g. Garrels and Mackenzie 1967; Drever and Finley 1993; Drever and Clow 1995; White and Blum 1995; Gislason et al. 1996; Oliva et al. 2003; White et al. 2005; Gislason et al. 2008, 2009). Surface water composition in the all-granitic area of the Maggia and Verzasca valleys in the Ticino of the Central Alps strongly depends on elevation (Drever and Zobrist 1992). Dissolved silica decreases exponentially from 252 to 15 μmol kg^{-1} SiO_2 as elevation increases from 360 to 2400 m a.s.l. TDS decreases by a factor of 8 along that section. The composition of stream water in the glacial granitic catchment of the Damma glacier area (Aar massif, Central Swiss Alps) shows significant variations in cation/Si ratios during the year. This variation can be related to different residence times of the water (Hindshaw et al. 2011). Low discharge in winter is associated with low cation/Si ratios and high discharge in summer produces water with high cation/Si ratios (Hindshaw et al. 2011).

Relatively few studies focused on ultramafic bedrock (or aquifers) (e.g. Barnes et al. 1967, 1972, 1978; Barnes and O'Neil 1969; Cleaves et al. 1974; Papastamataki 1977; Pfeifer 1977; Neal and Stanger 1983; Bruni et al. 2002; Marques et al. 2008). Typical waters from catchments with ultramafic rocks (peridotite and serpentinite) are Mg-HCO_3 type waters. Bruni et al. (2002) and Cipolli et al. (2004) reported spring waters from Genova, Italy, where both, neutral Mg-HCO_3 waters and high-pH Ca-OH waters are associated with serpentinites. Low-temperature serpentinization is also responsible for high-pH waters found in the ophiolite on Cypros (Neal and Shand 2002). Marques et al. (2008) noted that shallow Mg-HCO_3 groundwater in Central Portugal derived from interaction with the local serpentinized peridotite. Bucher et al. (2015) analyzed silica-rich Mg-HCO_3 surface water from catchments in the Ronda Peridotite in southern Spain. These studies emphasized that dissolution of Mg silicates (olivine and serpentinite) controls the water composition. Fast dissolving olivine may drive dissolved silica close to saturation with amorphous silica.

The contrasting compositions of surface waters resulting from water–rock interaction are linked to different solubility of minerals and the kinetics of weathering reactions (Lasaga et al. 1994; White and Brantley 1995; White et al. 2001). The source of a specific solute is difficult to relate to the dissolution reaction of specific minerals (e.g. Bassett 1997; O'Brien et al. 1997; Bricker et al. 2003; Velbel and Price 2007). The geogene composition of surface water from silicate rocks catchments generally represents a transitional non-equilibrium state influenced by mineral solubility and reaction rates (Garrels and Mackenzie 1971; Meybeck 1987; Bluth and Kump 1994; Drever 1994; White and Blum 1995; Oliva et al. 2003). The composition of water collected at a specific site (brook, pond) includes a number of dissolution and oxidation processes that were simultaneously in progress before sampling. By taking the water sample and separating the water from the reactant solids, the reactions are stopped and the water represents a specific progress of the overall reaction. Therefore, the chemical characteristics of surface water closely reflect the time integrated consequences of many chemical reactions in progress, which account for significant dissimilarities in water composition and weathering behavior of exposed rocks (Schnoor 1990; White and Hochella 1992; Drever and Clow 1995; White and Brantley 2003).

In the Zermatt area, a large variety of bedrocks are located in a relatively small size watershed (216 km^2 Zermatt; 35 km^2 Täschvalley). Within the watershed hydrologic parameters are relatively similar with the exception of elevation. External, non-geogene influence is minimal. Our study of high-altitude water chemistry is focused on water–rock interaction and the mechanism of weathering processes acting on exposed bedrocks.

2 Topography, hydrology and geology of the Zermatt area

The Zermatt area of the Swiss Alps (Fig. 1) is characterized by a rugged topography ranging from 1600 to 4600 m a.s.l. More than 20 peaks reach elevations above 4000 m including Matterhorn (4475 m). The tree line is at 2000 m and vegetation on soil ends at about 2700 m. The area is heavily glaciated and some major Alpine glaciers are located in the Zermatt region. The glaciers rapidly recede and new bedrock outcrops and vast moraine fields are

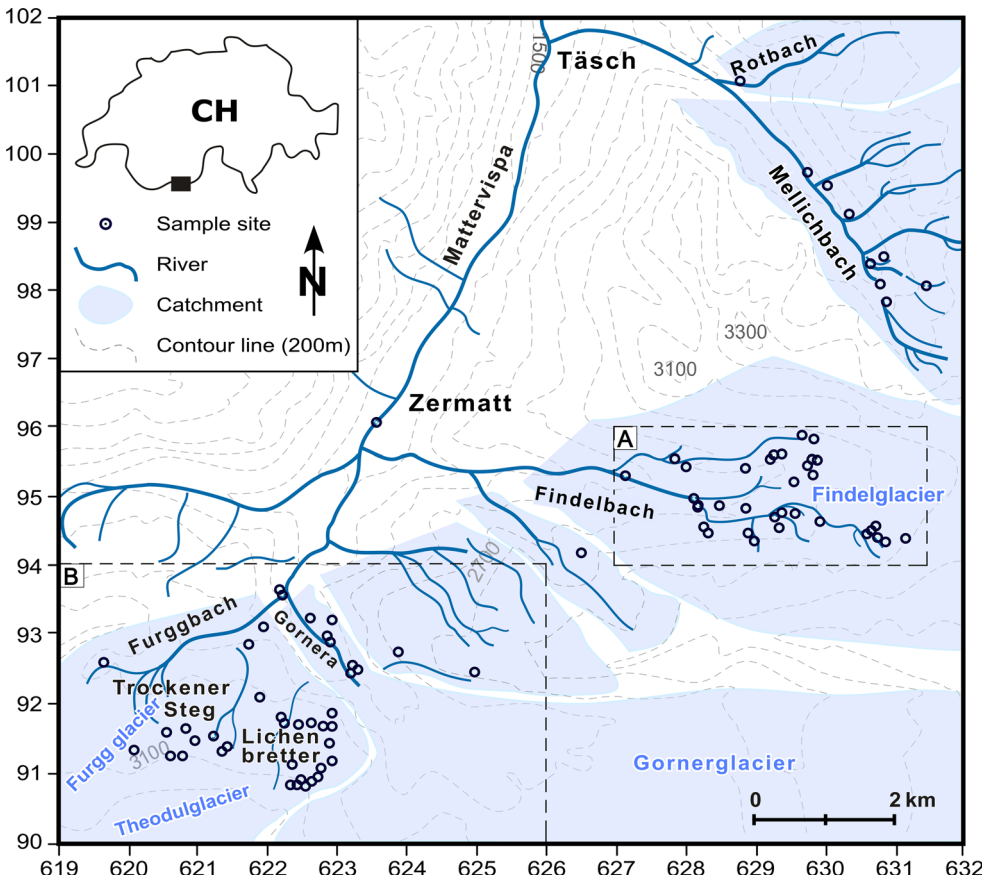

Fig. 1 Sample localities and outline of catchment areas (*blue shading*). Coordinates from the Swiss Coordinate km network (*numbers* refer to km from origin). Details of sub-area A Findelglacier are shown on Fig. 4, of sub-area *B* Trockener Steg and Lichenbretter on Fig. 6

released by the retreating ice masses every year. Findelglacier and Gornerglacier receded more than 2 km between 1882 and 2016. The hydrology of some of the glaciers has been studied and monitored and runoff data are available from glaciology studies (Maisch et al. 2004; Huss et al. 2007). This Alpine region is hydrologically characterized by moderate precipitation (mostly snow and rain), permanent runoff from the glaciers, a distinct snow melt period and sporadic rainfall in the warm season (Schwarb et al. 2001a). Hydrologic data are also available from long term monitoring programs (Schwarb et al. 2001b). Surface waters are steep fast running Alpine brooks that are well mixed with the atmosphere. The five main glaciers of the investigated area release runoff of meltwater that are collected by installations for hydroelectric power generation. The investigated catchments terminate at these water collectors and the respective elevations are (Table 1): Findelglacier 2500 m, Gornerglacier 2200 m, Täsch valley 2500 m, Zmutt glacier 2000 m. Surface runoff and shallow ground water have also been taken from below the hydroelectric water collectors. Strictly, these latter waters may have a significant anthropogenic influence. Much of the dilute high-altitude water disappears in the collectors and finally reaches the reservoir lake of Grande Dixence west of Zermatt. Most water samples of this study are from small water bodies upstream of hydroelectric installations, however, and are not chemically influenced by the power system. The collected samples represent typical surface water of the high mountain area of the Zermatt region. In recent years, the hydrology of the region has also been strongly influenced by the construction of water collecting ponds for making artificial snow during the skiing season. All water samples of this study are not affected by these anthropogenic actions with the exception of a few low elevation samples from the Gornera and the Trockener Steg area (Fig. 1).

The average monthly precipitation in Zermatt is about 58 mm and the annual average temperature is close to 3.5 °C (Fig. 2). Atmospheric dry deposition, either contained in snow or rain, or from dry deposition onto the catchment surface (Barrie 1991; Cadle 1991) may contribute solutes to surface water. The solute input from precipitation is given by the chemical data of rainwater and snowmelt water in and around Zermatt (Table 2). The rainwater samples from the Täsch valley near Zermatt (Bühring 2008) contain $CaSO_4$, NH_4NO_3 and NaCl (Table 2). The unusually high TDS of the rain (8 mg L^{-1}) can be explained by the short duration of the sampled rainfall event after a relatively long dry period. Ammonium nitrate contributes more than 50% of the TDS (by mass).

Table 1 Geology of the four regional catchments (Fig. 1)

Region	Geology	Snow, glacier cover	Catchment boundary	Vertical extent	Surface water	Bedrock lithology
Mellichbach	Mainly in the ZS ophiolite nappe, 6 km at NE of Zermatt	55% of watershed area of 25 km^2 is covered by several glaciers	Leiterspitzen, Kinhorn, Täschhorn, Alphubel, Allalinhorn, Rimpfischorn, Pfulwe	From 2200 m at Mellichbach to 4490 m Täschhorn	Spread several streams joining the main river Mellichbach	Eclogite, blueschist, serpentinite Rotbach subcatchment: paragneiss
Findelbach	ZSO on the N side; Monte Rosa on the S side, 6–11 km east of Zermatt	40% of watershed area of 37 km^2 is covered by Findelngletscher and other glaciers	Oberrothorn, Adlerhorn, Schwarzberghorn, Cima di Jazzi, Stockhorn and Gornergrat	From 2000 m at Findelnbach to 3803 m Cima di Jazzi	Spread small lakes and streams; one main river Findelbach	N side: metabasalt, serpentinite, calcareous micaschist, marbles, S side: granite, gneiss,
Trockener Steg	Mainly ZSO, 5 km at SW of Zermatt	50% of watershed area of 18 km^2 is covered by Theodulgletscher	Hirli, Matterhorn, Furgghorn, Theodulhorn	From 2200 m at Furggbach to 4477 m Matterhorn	Spread small lakes; one stream, Furggbach	E side: serpentinite W side: metabasalt, micaschist, marbles
Gornera	Monte Rosa and ZSO, 5 km south of Zermatt	80% of watershed area of 82 km^2 is covered by several glaciers which are tributary to Gornergletscher	Breithorn, Liskamm, Dufourspitze, Cima di Jazzi, Gornergrat	From 2005 m at the Gornera water intake to 4634 m Dufourspitze	Spread small streams; only one river, the Gornera	Granite, gneiss in MR nappe, serpentinite (Breithorn), metabasalt, calcareous micaschist and marble in lower part

ZSO Zermatt-Saas ophiolite nappe, *MR* Monte Rosa

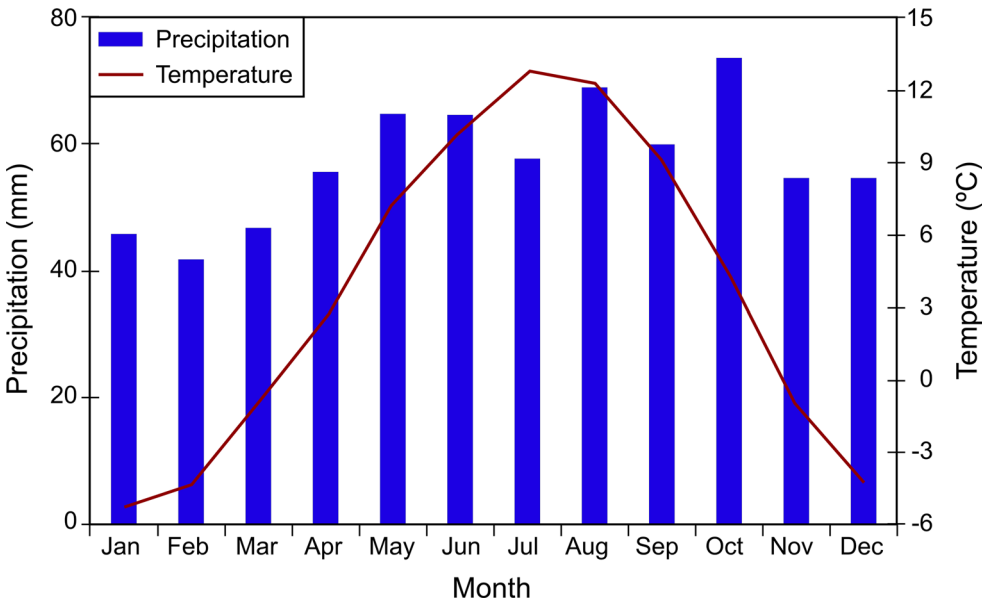

Fig. 2 Monthly average precipitation and temperature in Zermatt area. Source of data: Swissmeteo

TDS of the average annual precipitation in the Zermatt area is assumed to be close to 1 mg L^{-1}. Similar nitrogen data have recently been reported by Hiltbrunner et al. (2005) from alpine snow pack and rain from the Central Alps.

The key unit of the geology of the Zermatt region is the eclogite facies Zermatt-Saas ophiolite nappe (Fig. 3). It represents elements of the oceanic lithosphere of the South-Pennine basin of the Mesozoic Tethys Ocean. During early stages of Alpine orogeny, the oceanic lithosphere has been subducted to the mantle. Fragments of the oceanic material were returned to the surface as serpentinites, eclogites, eclogite facies metagabbro and metasediments (e.g. garnet-phengite schists). The rocks show that they have been subducted to 2.5–2.7 GPa corresponding to 70–80 km

Table 2 Chemical composition in atmospheric deposition

Location	Region	Type	Source	pH	Na	K	Ca	Mg	NH_4	Cl	SO_4	NO_3	TDS
Gornergrat	Zermatt	Snow	This study	5.65	0.08	0.07	0.38	0.05	n.a.	0.05	b.d.	0.46	1.63
Täsch valley	Zermatt	Rain	Bühring (2008)	5.47	0.24	0.06	0.67	0.05	1.06	0.17	1.52	3.59	7.81
Fieschergletscher[a]	Bernese Alps	Ice core	Jenk (2006)	n.a.	0.02	0.01	0.13	0.01	0.14	0.03	0.7	0.36	1.4
Fieschergletscher[b]	Bernese Alps	Ice core	Eichler et al. (2004)	n.a.	0.01	0.01	0.09	0.01	0.09	0.03	0.38	0.15	0.78
Grenzgletscher[b]	Zermatt	Ice core	Eichler et al. (2004)	n.a.	0.03	0.02	0.1	0.01	0.08	0.05	0.37	0.27	0.92
Col du Donon[c]	E France	Snow	Colin et al. (1989)	3.51	0.02	0.11	0.26	0.29	0.13	0.06	0.24	0.28	1.39
Col du Donon[c]	E France	Rain	Colin et al. (1989)	4.8	0.16	0.04	0.15	0.02	0.32	0.31	0.7	0.54	2.24
Lausanne[d]	W Switzerland	Rain	Atteia (1994)	n.a.	0.17	0.25	0.77	0.05	n.a.	0.48	0.72	0.43	2.87
Lausanne[d]	W Switzerland	Snow	Atteia (1994)	n.a.	0.38	0.19	0.54	0.03	n.a.	0.94	0.35	0.41	2.84
Freiburg	SW Germany	Rain	This study	5.27	0.02	0.06	0.52	0	0.34	0.1	0.61	1.25	3.47
"Initial water" used in the inverse models of this study[e]				5.53	0.18	0.06	0.57	0.05	0.68	0.13	0.98	2.48	5.62

Composition in mg L^{-1}

n.a. not available, *b.d.* below detection limit

[a] Average data from 1960 to 1990

[b] Average data from 1945 to 1983

[c] Average data from April to May, 1985

[d] Average data from 1990 to 1991

[e] Calculated data, see text

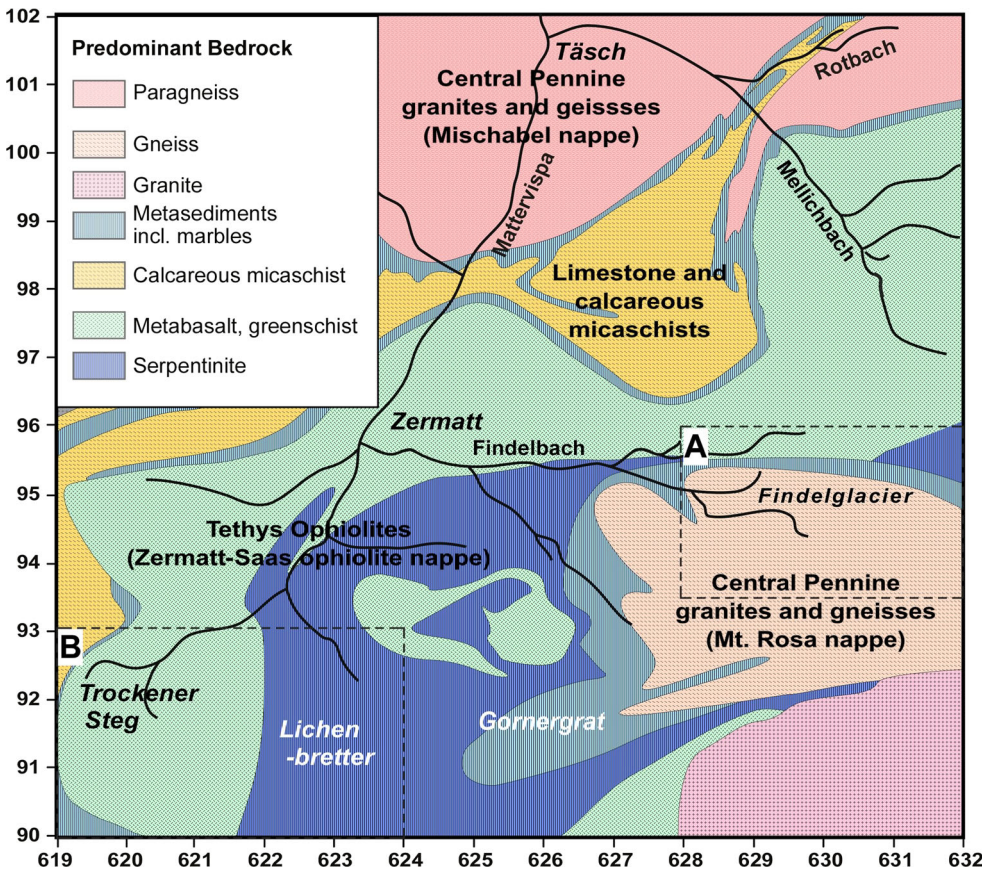

Fig. 3 Simplified geological map (after Steck et al. 1999) showing catchment and outcrop lithology in the Zermatt-Saas area. Penninic metasediments are predominantly calcareous micaschists in *yellow* (Tsaté nappe) and dolomite marble and quartzites in *light blue* (Cimes Blanche nappe)

depth (Bucher et al. 2005; Bucher and Grapes 2009). Palaeogeographically to the North of the Pennine basin and tectonostratigraphically under the Zermatt-Saas nappe are the Monte Rosa nappe and the Mischabel nappe, representing continental basement and its sedimentary cover. The Mischabel unit consists of a basement of orthogneiss (Randa gneiss) and metapelitic staurolite-garnet paragneiss building up the prominent Mischabel Mountains and forming the catchments in the northern part of the Täsch valley (Figs. 1, 4). The Monte Rosa unit is build up of prealpine basement including metagranites, gneisses and high-grade metasediments, migmatites and a Mesozoic metasedimentary cover of mostly detrital sediments. The entire nappe pile is overlain by the Dent Blanche nappe representing continental basement from the southern margin of the Tethys Ocean and the Piemonte oceanic basin. It is made up predominantly of granitoid gneisses in the Zermatt area forming the quite well known mountain Matterhorn among other prominent peaks.

The units of Penninic metasediments between the Mischabel nappe in the north and the Zermatt-Saas meta-ophiolite nappe (Fig. 3) are hydrochemically important. It is a complex unit of predominantly carbonate-rich metasediments and greenschist facies meta-ophiolites with poorly preserved relics of blueschist facies metamorphism (Tsaté nappe) and rare rootless relics of pre-Tethys Triassic metasediments (dolomite, quartzite) (Cimes Blanche nappe). The two nappes are rich in carbonate rocks located in particular catchments (Figs. 1, 3). Water from watersheds with calcareous metasediments is expected to be strongly influenced by calcite dissolution.

The sampling area can be subdivided into four larger main catchments (Figs. 1, 4, 5, 6): Trockener Steg, Gornera, Findelbach and Mellichenbach (Täschvalley). A large variety of different bedrocks from two or three major geologic units characterize the geology of these catchments (Table 1). However, the four regions can be further subdivided into several smaller catchments with a gradually more simple bedrock geology. Ultimately we sampled catchments underlain by a single rock type, which produce characteristic waters for the respective lithology.

Moraine cover is present in most catchments and much of the composition of surface water is probably acquired during the passage of precipitation or meltwater through unconsolidated moraine material (Fig. 5). It is therefore important to identify the predominant rock type of the moraine material. The material is derived from the bedrock geology of the glacier basins and the flow path of the ice. This may result in well-mixed moraines with rock debris from all units, monomict moraines with only one lithology present and in combinations of the two-endmember cases. Particularly critical is the content of carbonate rock debris (marbles, calcareous micaschists) in the moraine material due to the high solubility and fast dissolution kinetics of carbonate minerals as opposed to silicates. In the presented study, the rock material in the moraines has been recorded during our fieldwork and deduced from the geology of the glacier basins (geological maps: Bearth 1953, 1967; Bucher et al. 2003).

3 Sampling and laboratory methods

Two sampling campaigns were carried out in the fall of 2007 and 2008, respectively. The samples were mainly taken from small water bodies. The average altitude of the sampling points was around 2600 m a.s.l. that is above direct anthropogenic and biomass input. A few samples were also collected from the main rivers at lower altitudes

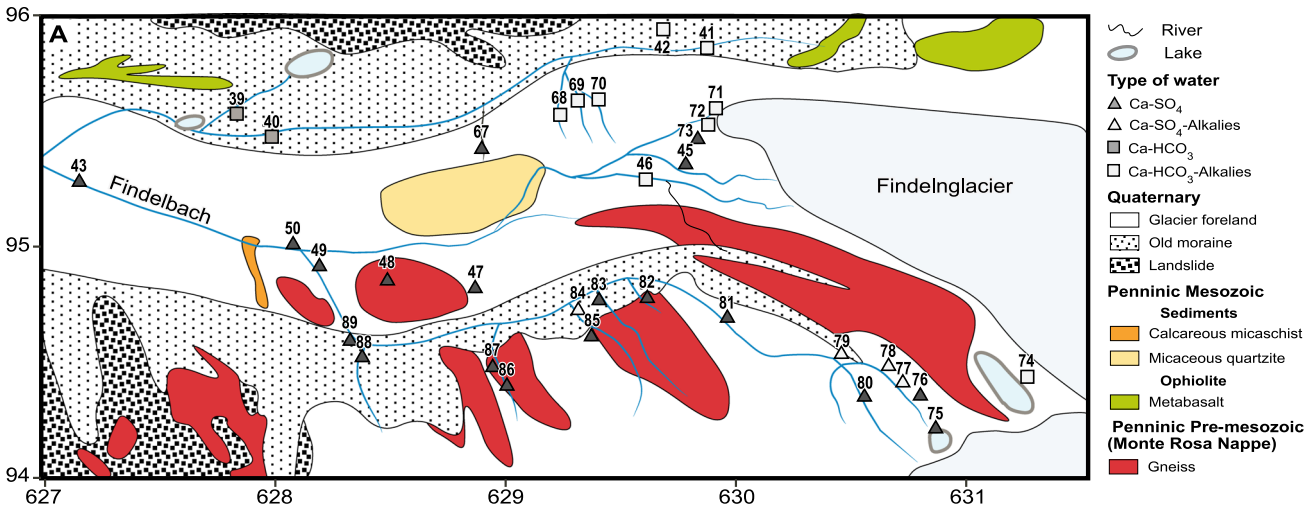

Fig. 4 Geology and hydrochemistry of the Findelbach catchments (area A of Fig. 1; geology after Bearth 1967). Coordinates from Swiss Coordinate System

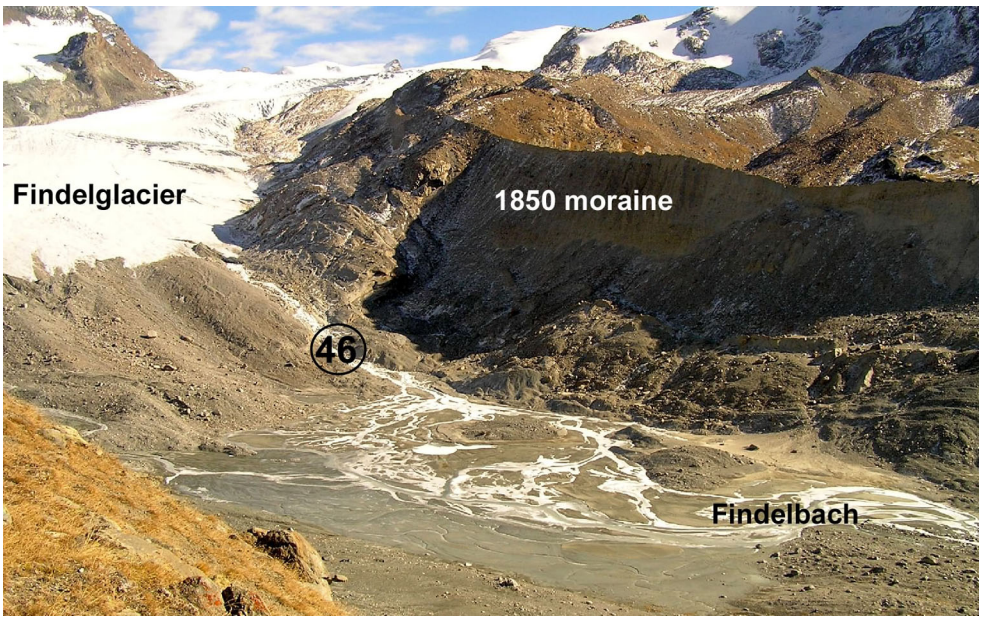

Fig. 5 View of the Findelglacier area looking SE in September 2008 (Fig. 1). The glacier river sampling site *46* (Fig. 4) is marked. Note braided river in the glacier foreland. Also note large outcrops of Monte Rosa gneiss (Fig. 4) recently released by the glacier. Above the prominent dark moraine are the sampling localities of many of the low-pH Ca-SO_4 waters (Fig. 4)

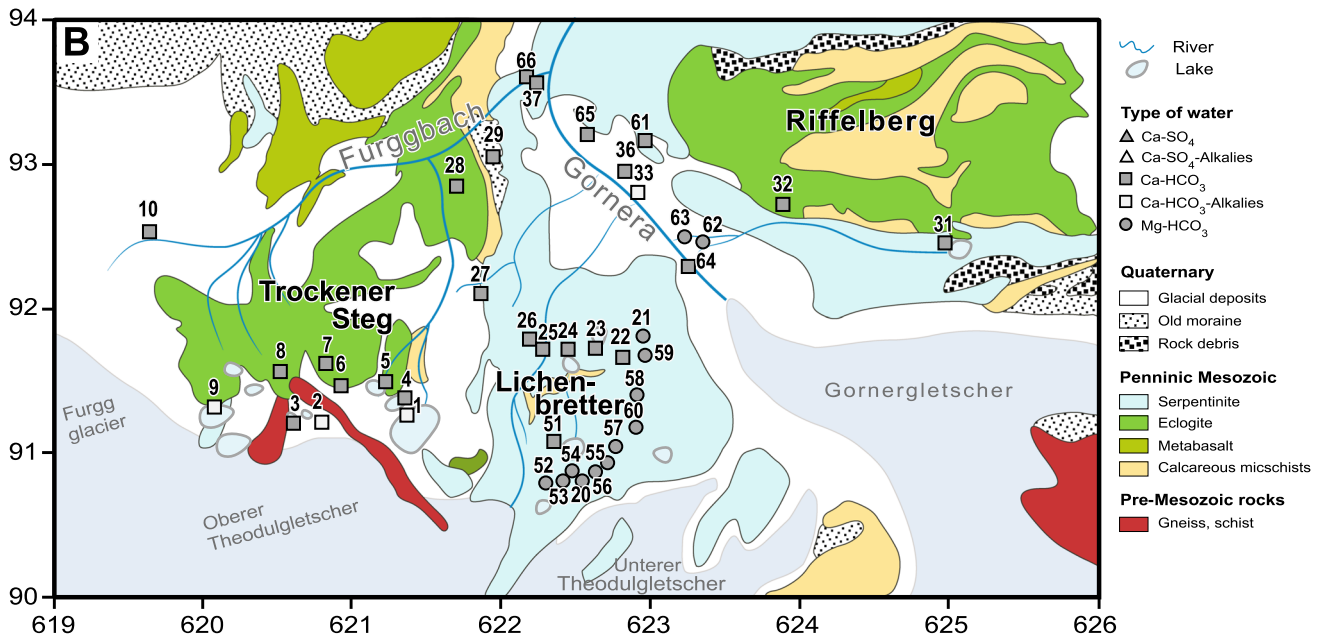

Fig. 6 Geology and hydrochemistry of the Trockener Steg and Lichenbretter catchments (B area in Fig. 1; geology after Bearth 1967; Weber and Bucher 2015). Coordinates from km-grid of Swiss Coordinate Network

(Zermatt 1600 m). The main rivers from the four principal catchments and the final mixing in the river Mattervispa below Zermatt characterize the overall chemical weathering.

87 surface water samples have been collected in pre-cleaned polyethylene bottles, which were washed three times by the sampled water. All the samples were stored in a refrigerator after sampling and transferred to the laboratory within one week. At each sampling site, water temperature, pH and electric conductivity (EC) of water were determined in the field by means of portable instruments.

All water samples were filtered by 0.45 µm filters before being analyzed. The cations Na^+, K^+, Ca^{2+}, Mg^{2+} and Sr^{2+} were analyzed by Atomic Absorption Spectroscopy

(AAS) with a precision better than 5% and the detection limits are (in mg L^{-1}): Na^+ 0.005, K^+ 0.01, NH_4^+ 0.01, Mg^{2+} 0.01, Ca^{2+} 0.02, Sr^{2+} 0.06. The anions SO_4^{2-}, Cl^-, NO_3^- were measured by Ion Chromatography and the detection limits are: SO_4 0.05, Cl 0.1, NO_3 0.01. Alkalinity (assumed equal to HCO_3^-) was analyzed by acidimetric titration and SiO_2 and NH_4^+ by UV/VIS spectrophotometry. The accuracy of the analysis was assessed by running 10 times standard samples at each analytical sequence (Online Resource 1). All AAS analyses have been repeated automatically three times and the other solutes have been analyzed two times to assure reproducibility. NH_4^+ has not been detected in any of the samples, therefore the total of dissolved solids (TDS) has been calculated from the analyzed concentrations from the equation: TDS (mg L^{-1}) = HCO_3 + Cl + SO_4 + Na + K + Ca + Sr + Mg + SiO_2.

The overall charge error of the analyses expressed as electroneutrality (EN) was calculated from (meq L^{-1}): EN = 100 × (sum of cations − sum of anions)/(sum of cations + sum of anions), concentrations in meq L^{-1}. The average EN for all 87 samples was around −4%. In 8 samples the EN was up to −15%, with the sum of anions exceeding the cations. High EN values were predominantly calculated for low TDS waters (all less than 20 mg L^{-1}), because small analytical errors may lead to high EN values. Also these samples were used for this paper.

CO_2 gas dissolved in the water expressed as log P_{CO_2} (Online Resource 1) was calculated from the equilibrium $CO_2 + H_2O = H_2CO_3 = H^+ + HCO_3^-$ and using the expression: log P_{CO_2} = log[HCO_3^-] − -pH + pK_{CO_2} + pK, the constants used pK_{CO_2} = 1.12, pK = 6.58 at 5 °C (Ford and Williams 1989). Average computed P_{CO_2} is slightly above atmospheric CO_2 (logP_{CO_2} = −3.2 instead of −3.45).

4 Results

4.1 Chemical composition of surface water

The composition data of all water samples are listed on Online Resource 1 (Electronic Supplementary Material (ESM) together with coordinates of the sampling localities.

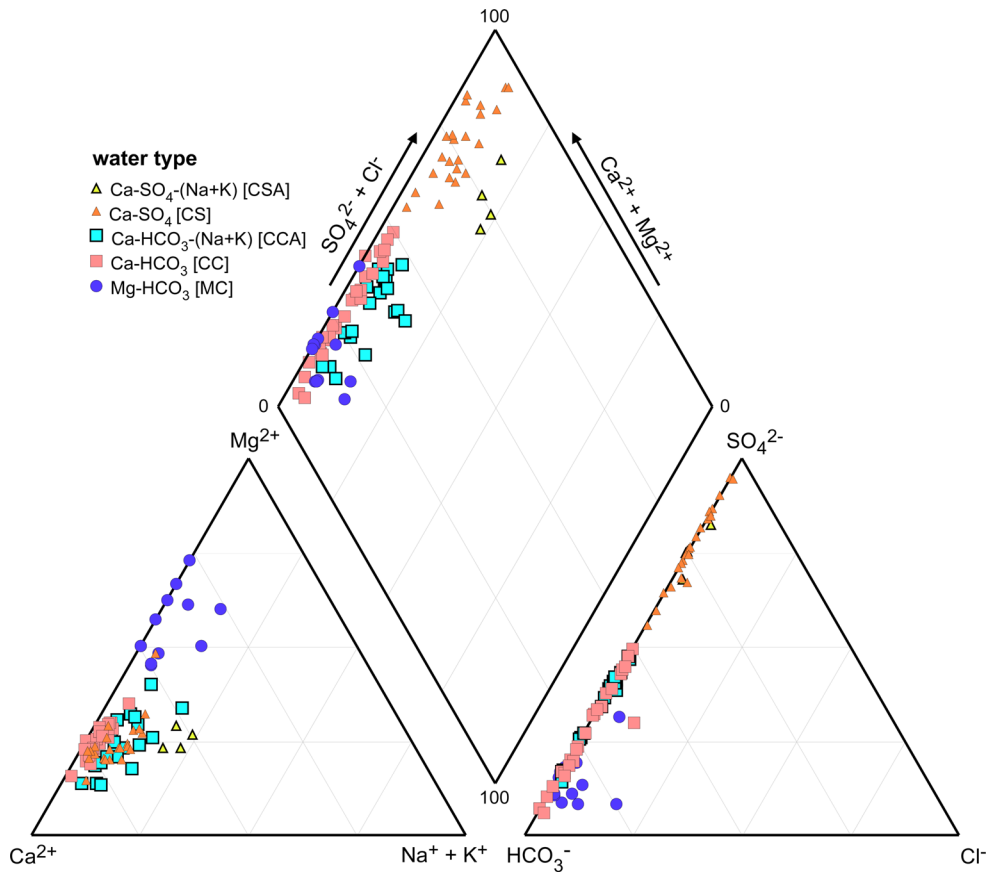

Fig. 7 Piper diagram of surface waters in Zermatt area: the data are in meq L^{-1}; *triangles* Ca-SO_4 water (CS), number of points (nop) = 20; *open triangles* Ca-SO_4 water with high alkalis (Na + K) (CSA), nop = 4; *square* Ca-HCO_3 water (CC), nop = 28; *open square* Ca-HCO_3 water with high alkalis (Na + K) (CCA) nop = 21; *circle* Mg-HCO_3 water (MC), nop = 13

The total mineralization of the waters ranges from 6 to 270 mg L^{-1}. TDS of the most dilute waters is similar to rain water composition (Table 2). The average TDS of all 87 samples is 86.1 mg L^{-1}. The highest mineralized waters show a solute load that is 80 times higher than that of local rain and the average concentration factor is 30.

The dominant cation of all waters is Ca^{2+} followed by Mg^{2+}. The average Ca/Mg mass ratio is 4.4 and only four low TDS samples from the serpentinite area of Lichenbretter are Mg dominated (Ca/Mg <1, molar ratio). K^+ is normally the dominant alkali metal and 80 of 87 samples have Na/K mass ratios smaller than one (average Na/K = 0.47 mass = 0.80 molar). All water samples contain a detectable trace amount of Sr^{2+} (up to 0.75 mg L^{-1}). Ca/Sr molar ratio varies from 4 to 2860.

Hydrogen carbonate HCO_3^- is the most abundant anion in most waters. It is followed by sulphate (SO_4^{2-}). The average mass ratio HCO_3^-/SO_4^{2-} is 3.44 and ranges from 0.06 to 20. Nearly all sulphate-dominated waters (HCO_3^-/SO_4^{2-} <1) were sampled from the Findel South and Findelglacier localities (Online Resource 1). The content of Cl^- is generally very low (maximum 0.81 mg L^{-1}) and nitrate (NO_3^-) (up to 1.50 mg L^{-1}) is 3 times higher on average than Cl. Dissolved Si (as SiO_2) ranges from traces to 8.31 mg L^{-1}.

4.2 Tagging the surface water

The data displayed on a standard Piper diagram form distinct groups both with respect to cations and anions (Fig. 7). From the distribution of the data, the chemical composition can be categorized into three main types: (1) Ca-SO_4, (2) Ca-HCO_3, and (3) Mg-HCO_3. The Ca-SO_4-rich and Ca-HCO_3-rich types of water can be further arranged into two sub-groups each on the basis of the abundance of alkali metals (Na + K) relative to the total of cations (Figs. 7, 8). Thus the notation used in this paper is: Ca-SO_4 (CS), Ca-SO_4-Na-K (CSA), Ca-HCO_3 (CC), Ca-HCO_3-Na-K (CCA) and Mg-HCO_3 (MC) water.

The defined water types clearly form five separate groups on the Piper diagram (Fig. 7). The Ca-rich waters vary little with respect to the cations; however, the Mg-rich waters form a distinct group (Fig. 7). Anion compositions spread along the low-Cl side of the anion triangle (Fig. 7) and cover the full range from HCO_3 to SO_4. On the anion triangle, MC water form a separate group because of a relatively high proportion of precipitation derived Cl and low TDS. There is a clearly distinguishable group of high sulphate water with sulphate greater than 50 meq % of the anions. This is particularly well visible on the rhombus of Fig. 7 where CS (orange triangles) and CSA (yellow triangles) occupy separate fields with no overlap. Also CC and CCA water occupy distinct field on the rhombus of Fig. 7. Both water types show a large HCO_3-SO_4 variation. The MC group serpentinite waters are all low in sulphate. From the Na versus K diagram (Fig. 8) it follows that all surface water are characterized by reactively high K/Na. On an average the molar K/Na is about 0.7. Particularly sulphate-rich water (CS and CSA) have K ~ Na or even K > Na (molar).

Molar calcium and hydrogen carbonate of CC and CCA water scatter around the 1:2 correlation reflecting the dominance of calcite dissolution (Fig. 9a). CS and CSA water contains a lot more calcium per HCO_3^- indicating another source for Ca^{2+} than calcite dissolution. In MC water Ca^{2+} is not related to carbonate (Fig. 9a). Magnesium increases with Ca in carbonate controlled water because calcite in marbles and calcareous micaschists contains irregular amounts of magnesite component (Fig. 9b). In CS and CSA water Mg does not correlate with hydrogen carbonate (Fig. 9b) except for four high TDS samples showing additional carbonate dissolution. Sodium is high in CCA and CSA water (by definition); however, it is also much higher in all sulfate water (CS) compared with the carbonate dominated CC waters (Fig. 10). Potassium shows a pattern very similar to sodium. Calcium correlates very strongly with TDS with the exception of CCA water, which scatter widely with TDS (Fig. 10). This is in sharp contrast to the magnesium diagram (Fig. 10d), where all water very strongly correlate with TDS. Hydrogen carbonate is the dominant anion in CC, CCA and MC water, sulphate in CS and CSA water (Fig. 10). This feature has been used for the definition of the water types.

The collected surface waters show distinct composition patterns on Schöller diagrams (Fig. 11). The pattern of the typical CC water type shows the predominance of earth alkaline metals and hydrogen carbonate (Fig. 11a). CCA waters (Fig. 11b) have a distinctly higher Na + K content than CC waters. The CS and CSA waters (Fig. 11c) are easily distinguished from the carbonate dominated waters by the steep sulphate branch of the pattern. Finally, MC waters (Fig. 11d) have the lowest TDS of all waters. The Ca/Mg ratio of MC water is lower than 1, whereas alkali metal and sulphate concentrations are lower than in other water types.

Further data on the Zermatt area water samples are given in the following grouped by the type of water:

CC and CCA water 49 samples are Ca-HCO_3-rich waters, including 28 CC waters with a TDS ranging from 51 to 244 mg L^{-1} and 21 CCA water with a TDS ranging from 43 to 185 mg L^{-1}. These CC and CCA types of water are from catchments dominated by metabasalt and metasedimentary bedrocks (Figs. 3, 4, 6). In the Täschvalley the tributaries of Mellichenbach (except Rotbach), the waters of the Northern Findelbach area, including the northern Moraine and the glacier waters of

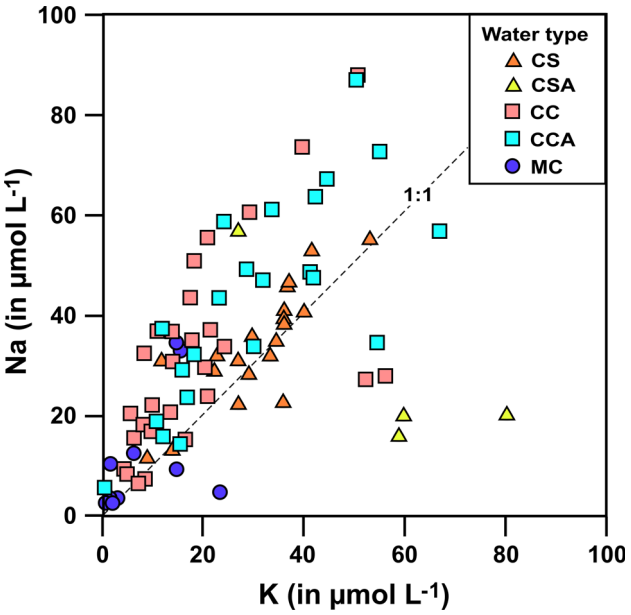

Fig. 8 Concentration of alkalis (Na + K) (mmol L^{-1}) versus total cations concentration (mmol L^{-1}) of all samples, *CS* Ca-SO_4 water, CSA = Ca-SO_4-alkalis water, *CC* Ca-CO_3 water, *CCA* Ca-CO_3-alkalis water, *MC* Mg-CO_3 water

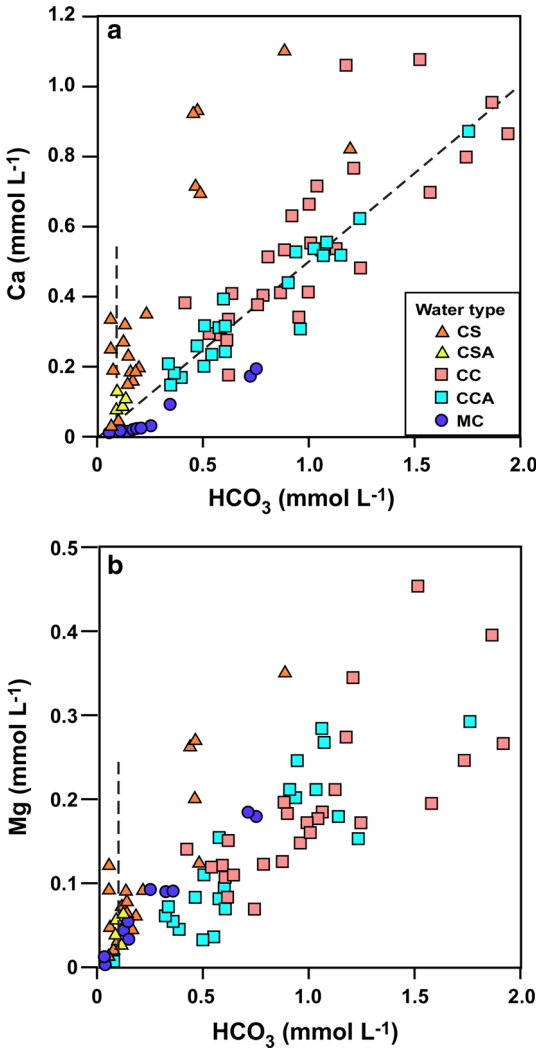

Fig. 9 **a** Calcium versus hydrogen carbonate; **b** magnesium versus hydrogen carbonate mmol L^{-1}; *CS* Ca-SO_4 water, *CSA* Ca-SO_4-alkalis water, *CC* Ca-CO_3 water, *CCA* Ca-CO_3-alkalies water, *MC* Mg-CO_3 water

the northern part of the Findelglacier area and the waters of Gornera and Trockener Steg are predominantly CC type waters (Figs. 1, 4, 6). Some of the CCA waters represent glacier runoff (Figs. 4, 6).

MC water 13 samples belong to the MC type with a TDS ranging from 6 to 66 mg L^{-1}. All MC waters have been collected from water bodies that have exclusively been in contact with serpentinite bedrock (Fig. 3, 6). The sampling localities have been in the Lichenbretter serpentinite region and in the Riffelberg serpentinite area belonging to the Gornera catchment (Fig. 6).

CS and CSA water 24 samples are Ca-SO_4-rich, including 20 CS water with a TDS of 16 to 269 mg L^{-1} and 4 CSA waters with a TDS of 29–40 mg L^{-1}. The CS and the CSA waters originate from catchments where bedrock, moraine and soil material is predominantly granite and gneiss (Figs. 3, 4). Except sample ZM19 from Rotbach (Täschvalley; Online Resource 1 and Fig. 1), all Ca-SO_4-rich water was sampled in the southern Findelbach catchment dominated by gneiss and granite of the Monte Rosa nappe (Figs. 1, 3). Also, CSA water, like CCA water, has been found in runoff from glaciers (Fig. 4).

4.3 Speciation and saturation states

The distribution of species and saturation states of the waters were calculated using the geochemical code PHREEQC (Parkhurst and Appelo 1999). The saturation index (SI) relates the ion activity product (IAP) to the equilibrium constant (K) of the dissolution reaction of a considered mineral at a given P and T: SI = log(IAP/K). SI is a useful measure for the distance from equilibrium of the water composition with respect to a selected mineral (Plummer et al. 1983; Parkhurst 1995; Drever 1997; Appelo and Postma 2007). Dissolution and precipitation of solids and the associated change in water composition is driven by the departure from equilibrium $\varsigma = 1 - (\mathrm{IAP/K})$. For all $\varsigma \neq 0$, the reaction proceeds in the forward or backward direction depending on the sign of ς (positive for dissolution, negative for precipitation).

All waters are undersaturated (SI < 0) with respect to all tested Al-free minerals that commonly occur in the assemblages of the bedrock, with the exception of quartz.

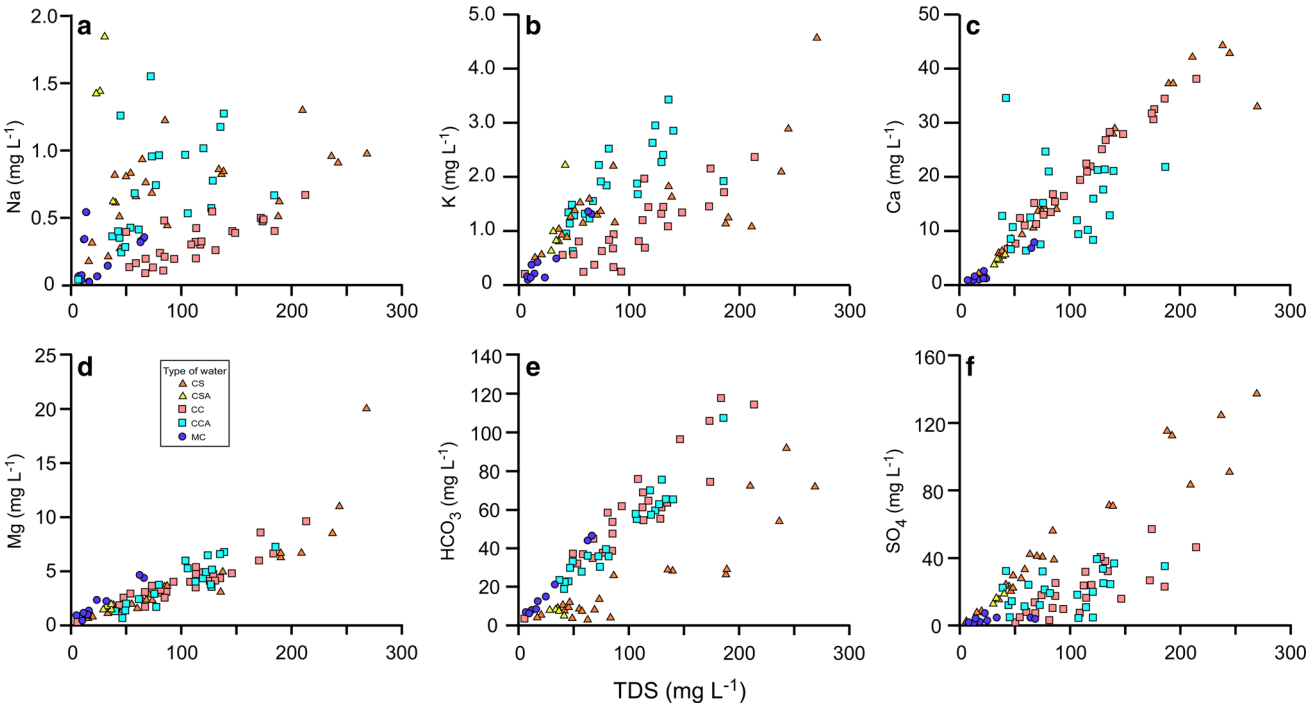

Fig. 10 TDS (mg L^{-1}) versus selected chemical composition parameters (mg L^{-1}). *CS* Ca-SO_4 water, *CSA* Ca-SO_4-alkalis water, *CC* Ca-CO_3 water, *CCA* Ca-CO_3-alkalis water, *MC* Mg-CO_3 water

The CS and CSA waters from South Findelbach and the Findelglacier are close to saturation with quartz ($-0.1 > SI_{Qtz} > 0.1$). The Findelglacier runoff is weakly oversaturated with respect to quartz. Undersaturation with respect to quartz ranges from SI = −0.2 to SI = −0.6 for the other water types. Surprisingly, none of the collected waters is saturated with calcite although calcareous micaschists dominate some of the catchments on the north side of Findelglacier. Water from Findelglacier and Trockener Steg has the highest SI_{Cal} of −0.65 to −0.53. However, because total dissolved aluminum cannot be analyzed due to its ultra-low concentration (<1 µg L^{-1}), the saturation state with respect to common primary and secondary silicates is unknown (feldspars, micas, chlorite, epidote, clay minerals, etc.).

5 Discussion

TDS of surface water increase from rainwater by an average factor of 30 (Table 2 and Online Resource 1). Unlike rainwater, sampled surface water contains no ammonium. In open systems, such as streams or lakes, NH_4^+ is oxidized to N_2 by O_2 and escapes from the water. Further oxidation of NH_4^+ to NO_3^- is low in the Zermatt surface waters (Online Resource 1). Ammonium has also not been detected in runoff from glacial sub-ice water. Higher sulphate in CS and CSA water than in rainwater indicates progress of reactions that supply sulphate together with associated cations from the bedrock. The concentrations of cations relate to the extent of reaction progress. In all Ca-rich water, both Ca and Mg show a more than 10 times higher concentration than the rainwater. In Mg-rich water chloride and nitrate concentration is similar in surface water and rainwater, suggesting that Cl and NO_3 are not increased by water–rock interaction. Thus Cl and NO_3 originate predominantly from atmospheric input.

An overview on the processes responsible for the development of the observed water compositions may be derived from the statistical correlation of the solute concentration data. This has been examined by cluster analysis using the Euclidean Distance measure of the software package SPSS 10.0. The cluster analysis groups data into discrete classes based on recurrent common attributes. The classes represent a relatively homogeneous feature within the group and also introduce the distinction from the others. In hydrogeology and hydrochemistry, cluster analysis is not primarily used for establishing cause-and-effect relationships, but rather for presenting data in such a way that cause-and-effect relationship can be deduced (Drever 1997). In this study, we used the method to compute the correlations among the chemical composition to assess sources of solutes and principal weathering processes. The data of eight solutes (Na^+, K^+, Ca^{2+}, Mg^{2+}, SO_4^{2-}, Cl^-, NO_3^-, Si), TDS, pH and temperature from all 87 samples have been input in the cluster analysis.

Table 3 Dissolution rate (R) in mol m^{-2} s^{-1}, 25 °C, pH 5. Revised from Lasaga (1984), Lasaga et al. (1994), Drever and Clow (1995), White and Brantley (2003)

Mineral	logR	References
Quartz	−13.4	Rimstidt and Barnes (1980)
Kaolinite	−13.3	Nagy et al. (1991)
Muscovite	−13.1	Lin and Clemency (1981)
Epidote	−12.6	Rose (1991)
K-feldspar	−12.4	Blum and Stillings (1995)
Albite	−12.3	Burch et al. (1993)
Biotite	−12.2	Acker and Bricker (1992)
Gibbsite	−11.5	Nagy and Lasaga (1992)
Chrysotile	−11.4	Bales and Morgan (1985)
Diopside	−10.2	Schott et al. (1989)
Enstatite	−10	Schott et al. (1989)
Forsterite	−9.5	Blum and Lasaga (1988)
Chrysotile	−8.6	Hume and Rimstidt (1992)
Anorthite	−8.6	Fleer (1982)
Wollastonite	−8.0	Rimstidt and Dove (1986)
Dolomite	−6.6	Wollast (1990)
Calcite	−5.1	Wollast (1990)

The cluster analysis shows that distinct pairs or groups of input parameters are markedly correlated (Fig. 12). There is a clear correlation of sulphate with Ca and Mg (Fig. 12) suggesting that the process that releases SO_4 into the waters also adds Ca and Mg. In the studied Zermatt catchments, there are no known rocks including the Triassic dolomite marbles of the Cimes Blanche nappe that contain minerals of the system $CaSO_4$–$MgSO_4$ (gypsum, anhydrite or $MgSO_4$ salts) or any other sulphate mineral that could produce the SO_4-rich water. Thus, the various sulfide minerals present in the rocks are the only sources of sulphate (Fig. 13). The most abundant sulfides in gneisses and schists of the Zermatt area are pyrite and pyrrhotite, but we frequently also found galena, sphalerite and chalcopyrite. Field evidence for active sulphide dissolution and Fe oxidation is rusty patches around pyrite in contact with the atmosphere and precipitation (Fig. 13). Outcrops of pyrite-rich schists become covered with Fe-hydroxide rinds in less than 5 years after being uncovered by ice-melt and glacier retreat. The oxidation reaction of pyrite, the most widespread sulfide phase in the bedrocks, can be written as:

$$4FeS_2 + 15O_2 + 14H_2O = 4Fe(OH)_3 + 8SO_4^{2-} + 16H^+. \quad (1)$$

Sulfide and Fe^{2+} are oxidized to sulphate and Fe^{3+} that is insoluble under surface conditions and precipitates as an iron hydroxide phase. Protons that are produced in the process potentially promote dissolution of other solids. Since sulphate is associated with Ca and Mg (Fig. 12), these cations are acquired by secondary processes that neutralize the sulfuric acid produced by the sulfide oxidation reaction (1). As a secondary effect of sulphide weathering dissolved CO_2 is slightly above equilibrium with atmospheric CO_2 because the lowered pH from reaction (1) increases calcite solubility.

The low level correlation between Ca and Mg and HCO_3 (Fig. 12), reflects the contribution from dissolution of carbonate minerals. At the surface, calcite and dolomite dissolve and react rapidly with atmospheric CO_2 (e.g. Wollast 1990; Drever and Clow 1995). In the Zermatt area, carbonate minerals are abundant in calcareous micaschists and in Triassic dolomite marble (Fig. 3). However, greenschists, eclogite, gneiss and granite also contain locally small amounts of secondary calcite and other carbonate minerals that formed during cooling and retrogression (Bucher et al. 2005; White et al. 2005; Bucher et al. 2009).

Alkali metals (Na + K) are highly correlated with dissolved silica (Fig. 12). It indicates that most of the alkalis were contributed to the water from reaction with Na- and K-bearing silicate minerals. Silicate dissolution is facilitated primarily by sulfuric acid generated by sulfide oxidation but also by carbonic acid from contact with the atmosphere. Solutes from the atmospheric input (Cl and NO_3) form a distinct group and they are weakly correlated with the alkalis (Fig. 12). The small amount of alkalis from atmospheric input is balanced with Cl and NO_3.

Finally, pH mainly correlates with temperature and not with any of the solutes. Temperature and pH are weakly correlated with TDS. It indicates that temperature influences the kinetics of the acid–base reactions that create the chemical characteristic of surface water.

At a first glance it appears surprising that pH and HCO_3 are weakly correlated. The reason for this can best seen on Fig. 10e. HCO_3 is linearly correlated with TDS for all but the CS and CSA waters. The later group damages the existing correlation for the CC, CCA, and MC waters. This has the effect that on the cluster diagram Fig. 12, HCO_3 and pH are only weakly correlated. On a HCO_3 versus pH diagram the two parameters correlate very well for the CC, CCA and MC waters but not for CS and CSA waters.

The water composition data show a remarkably consistent correlation with the bedrock lithology of the respective catchment areas. This central observation underlines that the water composition is primarily controlled by the reactions of precipitation water, mostly rain and snowmelt, with the exposed minerals of the bedrocks. The documented contrasts between the compositions of the water from the different sampling localities can be related to the different mineral assemblages present in the bedrocks of the local catchments. Therefore, the water composition

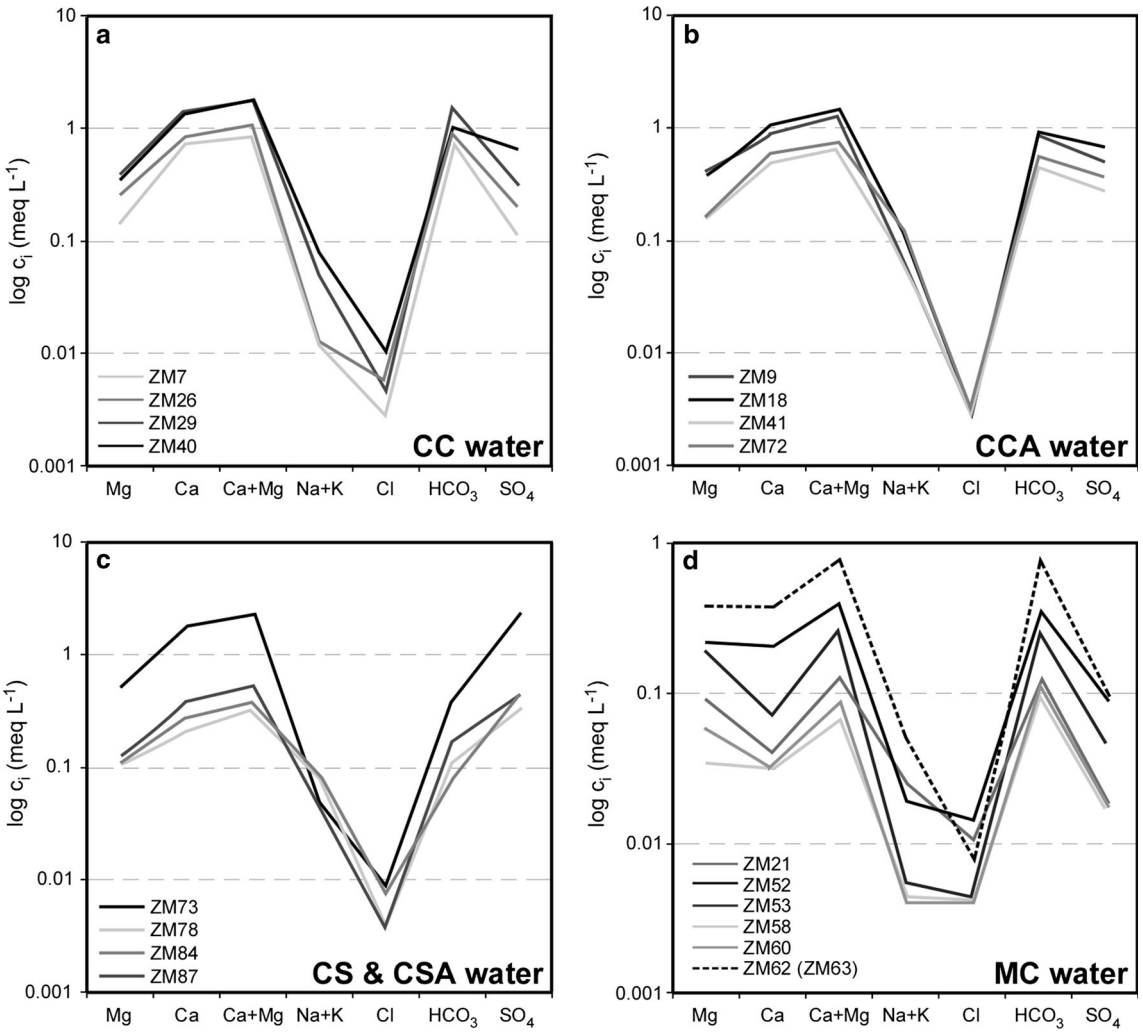

Fig. 11 Schöller diagram showing the concentrations of major solutes (c_i) in selected surface water expressed as $\log c_i$ in meq L^{-1}. Water types: **a** CC ($Ca\text{-}CO_3$) water, **b** CCA ($Ca\text{-}CO_3$-alkalis) water, **c** CS ($Ca\text{-}SO_4$) water (ZM73 and ZM87) and CSA ($Ca\text{-}SO_4$-alkalis) water (ZM78 and ZM 84) water, **d** MC ($Mg\text{-}CO_3$) water

needs to be related to the dissolution of specific minerals and groups of minerals.

The candidates for mineral sources for Na, K and Si are feldspars and micas including muscovite (phengite), paragonite and biotite. Rate constants for the dissolution of abundant rock forming minerals are listed in Table 3. It follows from these data that the expected prime source for K is K-feldspar and biotite and for Na albite. White mica dissolves considerably slower than the feldspars and biotite. The observed Na/K molar ratios (Fig. 8) between 1 and 2 are consistent with the listed similar rate constants for the two feldspars. All waters are far from equilibrium with respect to the common minerals of the bedrock. Although the overall rate depends on many factors, the dissolution is likely to occur on the dissolution plateau where, far from equilibrium, the rate is constant and independent from the affinity of the reaction (Lasaga et al. 1994).

The initial phase of dissolution of feldspars, mica or any other dissolving mineral in low TDS water is congruent dissolution. Congruent dissolution proceeds until critical supersaturation with respect to a product phase (e.g. kaolinite) is reached. From then on dissolution of primary minerals such as feldspar, mica or pyrite is incongruent. Pyrite dissolution (Eq. 1) produces a secondary Fe-hydroxide mineral and the processes is incongruent dissolution.

The composition of water is the result of many reactions running simultaneously at different rates including the dissolution reactions of Kfs, Pl, Qtz, Bt, Ms, Cal, Chl, Py and many other minerals found in the rocks coming in contact with e.g. rainwater but also all precipitation reactions forming secondary minerals such as various clays and Fe-hydroxides. It also includes all gas exchange reactions between the waters and the atmosphere and many other reactions. The overall reaction is the net effect of all these

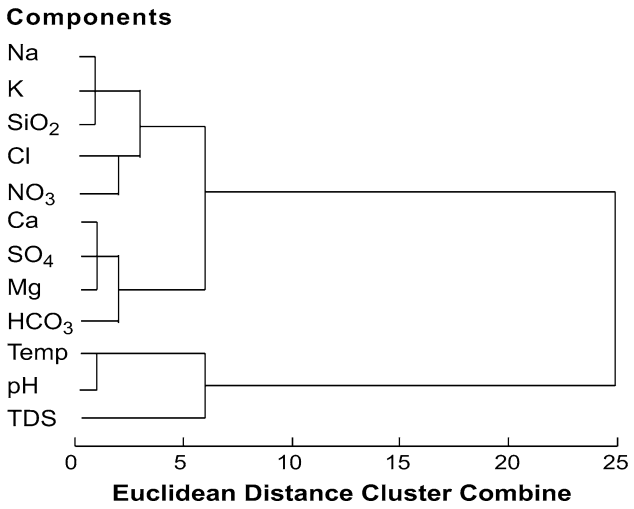

Fig. 12 Cluster analysis of all solute concentration, pH and temperature data

progressing reactions taken together and can be summarized as chemical weathering.

As the overall reaction progresses the water gradually increases in TDS until critical oversaturation with respect to low temperature minerals is reached and product minerals begin to precipitate. The individual incrongruent dissolution process is schematically:

$$\text{Initial water} + \text{reactant minerals} = \text{final water} + \text{product minerals}. \quad (2)$$

If the water becomes oversaturated with respect to a defined solid phase this phase does not form at affinity = 0. Rather it requires a certain affinity > 0 where heterogeneous nucleation begins and the phase starts growing at a finite rate. This affinity is known as critical oversaturation.

The composition of the initial water is known from rainwater and snow water analyses (Table 2). The reactant minerals of the bedrock in the catchments are also known. The composition of the final water corresponds to the water data set of this study. The identification of product minerals of reaction (2) is difficult and only few composition data for products are available. If the compositions of all solid and liquid phases participating in reaction (2) are known, the reaction stoichiometry can be balanced. The mass balance coefficients for specific formulations of Eq. (2) can be derived from different techniques (Velbel 1985; Taylor and Velbel 1991; O'Brien et al. 1997; Bowser and Jones 2002; Bricker et al. 2003; Tardy et al. 2005; Velbel and Price 2007; Price et al. 2008).

The minerals participating in the process must be added (dissolved) to or removed (precipitated) from the solution by reactive mass transfer. Inverse models solve a set of linear equations that account for the changes in the moles of each element by the dissolution or precipitation of minerals that occur as water evolves along a flow path (Garrels and Mackenzie 1967; Plummer and Back 1980; Parkhurst et al. 1982; Plummer et al. 1991). Inverse models for the Zermatt waters were computed with the geochemical code PHREEQC (Parkhurst and Appelo 1999) using precipitation data (Table 2) and measured mineral composition data for the Zermatt bedrocks (e.g., Cartwright and Barnicoat 2002; Li et al. 2004, 2008; Bucher et al. 2005; Weber and Bucher 2015). The product minerals of the alteration or weathering reaction (2) have been analyzed by x-ray diffractometry of clay sediments in the muddy foreland of Lichenbretter and Findelglacier. The dominant clay is kaolinite and it occurs with other newly formed alteration products, including illite, K-beidellite and Fe-hydroxides. These alteration products are similar to products of low-T hydrothermal alteration of the rock types relevant for the Zermatt area (Meunier and Velde 1982; Drever and Zobrist 1992; Sequeira Bragam et al. 2002; Bartier et al. 2008) The computed inverse models produce stoichiometric coefficients for the inferred specific reactions producing the five different types of water. The results depend on the chosen set of reactant and product minerals and are thus not unique. However, important generalized results from models with different sets of input reactant assemblages can be derived and are summarized in the following:

The inverse models show that non-atmospheric chloride input to all waters is negligible. The computed mass transfer coefficients were particularly sensitive to the composition of reactant plagioclase and biotite for reactions involving these minerals (see also Bowser and Jones 2002).

CC water: Catchments with prevalent CC waters contain abundant calcareous micaschists and Triassic marbles. Dissolution of calcite dominates solute acquisition. Depending on the sulphate concentration, pyrite dissolution and oxidation of Fe^{2+} to Fe^{3+} consuming O_2 is essential for the total mass transfer. Silicates are essentially not involved in the transfer process. The small amount of NaCl is exclusively contributed by atmospheric input.

CCA water: In addition to the dominant calcite dissolution and a considerable contribution from sulfide oxidation and dissolution, silicate weathering is important for generating CCA waters in catchments poor in carbonate rock. The principal bedrock of the catchments Mellichenbach, north Findelbach and west Trockener Steg is metabasaltic mafic schist containing albite, epidote, chlorite, phengite, actinolite and some sulphide. The catchments produce Na-K-Ca-HCO_3 waters (CCA). In models CCA water formed by a calcite-absent process involves only silicates and sulphide but no carbonate minerals. Epidote and actinolite dissolution can be a source of calcium in the

Fig. 13 Fe-hydroxide halos around rapidly weathering Fe-sulfide grains in garnet-phengite schist of the Trockener Steg area (Fig. 1). The outcrop has been released unstained by the Theodul glacier two years before the photograph has been taken

water. CCA water is related primarily to the glacier outflow. This is also the case for CSA water (see below).

MC water: Serpentinite is the dominant rock of the MC catchments. It contains antigorite (serpentine), forsterite, diopside, chlorite, magnetite and some accessory minerals (Li et al. 2004). The serpentinites contain various primary sulphides including pentlandite as source for sulphate in the waters. Since no potassic and no sodic minerals are present in serpentinites we assume that the very small amount of Na and K result from atmospheric input (rain, snow, dry deposition). Serpentine dissolution closely describes the observed composition of MC water.

$$Mg_3Si_2O_5(OH)_4 + 6CO_2 + H_2O = 3Mg^{2+} + 2SiO_{2aq} + 6HCO_3^- . \quad (3)$$

MC water is strongly undersaturated with respect to chrysotile and reaction (3) is far from equilibrium. They also remain undersaturated with respect to magnesite. Diopside may be the source of Ca in most of the MC samples instead of secondary calcite, which is present in some serpentinites. The generally low TDS of MC waters and the dominance of the cation Mg, which undeniably originates from a silicate (serpentine) dissolution reaction, suggests that also Ca is contributed by a kinetically slow silicate dissolution reaction. Also the low Ca/Sr ratio of MC water supports a silicate source for Ca. If calcite would be present, its high solubility (compared to silicates) would probably dominate water composition also in serpentinite catchments.

Locally, the serpentinites contain abundant metamorphic olivine of pure forsterite composition (Li et al. 2004). In such catchments much of the Mg in MC waters may originate from the kinetically relatively fast forsterite dissolution. This process can be described by model:

$$\text{Olivine-serpentinite: Initial water} + CO_2 + O_2 + \text{forsterite} + \text{diopside} + \text{pyrite} = \text{serpentine} + \text{goethite} + \text{Mg-}HCO_3\ \text{water}. \quad (4)$$

Reaction (4) describes MC water production essentially by serpentinization of forsterite. The mass transfer from ultramafic rock is significantly higher in the presence of forsterite compared with simple dissolution of serpentine because of the much higher kinetic rate constant of forsterite than chrysotile (Table 3). The iron-content of forsterite and serpentine is very low and can be neglected (Li et al. 2004). Dissolution of iron-bearing olivine has been identified as a mechanism for the formation silica-rich Mg-HCO_3 surface waters and of brown weathering rinds on the Ronda Peridotite in southern Spain (Bucher et al. 2015). The olivine-bearing serpentinites of the Lichenbretter area have only been partially coated with very thin brown rinds (1 mm) after being exposed to the atmosphere for hundreds of years. Serpentinites that have been exposed by the rapid glacier retreat during the last 30 years are still green and not covered by any recognizable weathering rind. This is in sharp contrast to the complete brown rind covering sulfide-

rich garnet-phengite schists near Trockener Steg (Weber and Bucher 2015). These rinds formed in less than 6 years exposition to the atmosphere (Figs. 5, 13).

CS water: Sulphate dominates the anion composition of Ca-SO_4 water occurring especially in the south Findelbach catchment. Oxidation and dissolution of sulfide is the source of SO_4^{2+}. Atmospheric sulphate input is negligible. CS waters drain gneiss and granite catchments. The surface of the bedrock is free of carbonates and exposes plagioclase, K-feldspar, quartz and mica (biotite and phengite) to the water. Some of the Monte Rosa basement rocks of the south Findelbach catchment also contain hornblende and cordierite–sillimanite gneisses occur in the north slope of the Stockhorn ridge that forms the southern boundary of the south Findelbach catchments. Trace amounts of apatite and, locally, epidote are present in the granites and gneisses as additional potential sources of Ca in the water. No carbonate-bearing schists or marbles are present in the catchment. The main source of the prime cation calcium is the weathering of plagioclase. Primary pre-Alpine plagioclase in the Monte Rosa basement rocks contains 20–40 mol% anorthite component. Conversion of oligoclase to kaolinite results in a water with $X_{Ca} = 0.2$ (molar Ca/(Ca + Na)). The Zermatt waters (Online Resource 1), however, have $X_{Ca} > 0.9$, except CSA water. Thus, there must be a sink for Na, or alternatively, an other source for Ca. Oliva et al. (2004) suggested that much of the Ca in water from a high-altitude granitic watershed in the French Pyrenees originates from dissolution of Ca-minerals that are present in trace amounts in the bedrock (e.g. epidote, titanite, apatite). However, epidote has a dissolution rate much smaller than Ca-bearing plagioclase (Table 3). Albite in fractures and on crusts suggests that the dissolution of the Ca-feldspar produces kaolinite and secondary albite feldspar. This albitization process is formulated with oligoclase in Eq. (5):

$$\begin{aligned}&\text{Plagioclase} + 2H^+ + H_2O = \text{kaolinite} + 4\text{albite} + Ca^{2+}\\&CaNa_4Al_6Si_{14}O_{40} + 2H^+ + H_2O = Al_2Si_2O_5(OH)_4\\&+ 4NaAlSi_3O_8 + Ca^{2+}.\end{aligned} \quad (5)$$

Primary plagioclase in Monte Rosa basement rocks range from oligoclase to andesine. Mass transfer coefficients for alteration reactions strongly depend on the composition of plagioclase (Bowser and Jones 2002). The protons for plagioclase dissolution (5) are provided by the pyrite oxidation process (1). CS waters are distinctly acid waters with pH between 5 and 7 (Online Resource 1), suggesting the efficiency of reaction (1) in the weathering process. The acidity produced is not buffered by the presence of calcite or other carbonates in the south Findelbach catchment.

Plagioclase dissolution and pyrite oxidation are two competing processes that may balance in a pH-conserving steady state (6):

$$\begin{aligned}&8\text{plagioclase} + 4\text{pyrite} + 15O_2 + 18H_2O\\&= 4\text{goethite} + 32\text{albite} + 8\text{kaolinite} + 8Ca^{2+} + 8SO_4^{2-}.\end{aligned} \quad (6)$$

The mass balance (6) describes the overall process that produces CS waters very well.

The presence of andesine and oligoclase in Monte Rosa gneiss and granite is in contrast to the rocks of the Zermatt-Saas ophiolite nappe, which contain only Alpine albite and primary igneous calcic plagioclase is absent. Plagioclase dissolution and oxidation and dissolution of primary iron sulphides provide calcium sulphate to the water leaving behind albitized plagioclase and goethite. Because of the relatively high proportion of sulphate-produced brown patches of Fe-hydroxide and brown weathering crusts on the rocks are common and typical of the bedrocks in catchments that generate CS and CSA waters (Figs. 5, 13).

CSA water: The CSA waters (Online Resource 1 and Fig. 7) are distinctly different from the CS waters and have characteristically higher alkalis than the later (relative to the low TDS). Also, CSA water, in the same way as CCA water, has been found in runoff from glaciers (Fig. 5). Similar relationships were found in runoff from Alaskan glaciers (Anderson et al. 1997, 2000). The cause of high alkalis and the dominance of potassium have been related to cation-leaching of biotite. However, runoff from glacier has been isolated from atmospheric CO_2, which reduces carbonate dissolution. This explains the generally lower TDS of CSA water and the increased K and Na relative to Ca. In addition, also atmospheric O_2 has reduced access under the glacier ice, which reduces sulphide dissolution and oxidation. Thus the relative increase of alkalis in CSA (and CCA) water must have another cause than direct mica and feldspar dissolution (or cation leaching) (Brown 2002). We propose that the alkalis result from enhanced ion exchange $Ca^{2+} \Leftrightarrow 2\ K^+$ (Na^+) on the newly formed ultra fine-grained product clay minerals, predominantly kaolinite, under the glacier ice (glacier mud). This process is far less efficient on solid bedrock surfaces directly exposed to the atmosphere. Mechanical grinding of rocks by glacier ice and the reaction of the suspended rock powder with sub-ice water partly compensates the lowered reaction rates due to high pH by the increased reactive-surface contribution. The fine-grained rock powder produced by ice-grinding results in sediments in the glacier foreland that is highly reactive and weatherable (Anderson et al. 1997, 2000). Evidence for ion-exchange between sub-glacial lake water and sediment has been found in the sub-glacial lake Whillans, Antarctica (Michaud et al. 2016).

The lake Whillans water, however, carries a significant seawater component and the reported ion-exchange removes Mg^{2+} from the water. Sub-ice silicate weathering at lake Whillans is characterized by long residence time and by biotic assistance of the weathering process (Christner et al. 2014; Michaud et al. 2016). Interestingly, relatively high alkali concentration has been related to the long residence time of the water. This is in contrast to the Zermatt water where high alkali is related to an active dynamic high Alpine weathering environment supported by active mechanical weathering but characterized by short residence time and cold temperatures (the process is not important in deep warm or hot waters in the upper crust). Glacial sediment weathering may be assisted by biological heterotrophic activity producing CO_2 and releasing Ca^{2+}, K^+ and HCO_3^- from carbonate and silicate dissolution to the water. Such a mechanism has recently been reported from cryoconite holes on Antarctic glacier surfaces (Bagshaw et al. 2016).

Sub-ice weathering has been studied at Haut Glacier d'Arolla west of the Zermatt area (Tranter et al. 2002). The solute load of the sub-glacial water reflects the weathering of bedrock in the upper glacier basin of Haut Glacier d'Arolla. It is dominated by paragneiss of the Arolla Series and abundant high-grade marble (Bucher et al. 2003, 2004). Metamorphic mafic rocks contribute little to the solute load at the borehole array where the waters have been sampled. Granitic gneiss of the Bouquetin Mountains may have added solutes to some waters, however, this remains unclear. The partially sulphate-rich waters indicate that sulfide-oxidation is, similar to the Zermatt area, an important process of solute acquisition. The oxidation proceeds until the environment progresses into anoxic conditions. It has been suggested that Fe^{3+} may become a significant oxidation agent in O_2 deficient sub-ice water (Raiswell et al. 2006).

Limited access of atmospheric O_2 (and CO_2) under the glacier ice is clearly demonstrated by initially lacking oxidation halos around sulfide grains at bedrock outcrops in the Zermatt area that have exposed by the rapid glacier retreat during the last 50 years. The fresh unoxidized sulfide grains at the rock surface can be interpreted as petrologic evidence for anoxic conditions under the glaciers or the brown Fe^{3+} hydroxide-oxide halos may have been removed by reduction of Fe^{3+}. No direct evidence for active Fe^{3+} reduction such as massive rusty crusts at water outlets by re-oxidation after contact with atmospheric O_2 is present in the Zermatt area. However, Fe^{3+} hydroxides may occur as unnoticed nano and micro clusters associated with clay (Raiswell et al. 2006). Limited CO_2 may provide by biogeochemical processes under the ice (Wadham et al. 2010). Water saturated with atmospheric O_2 can produce a maximum of about 80 mg L^{-1} sulphate if isolated from the atmosphere in a closed system batch reaction of sulfide oxidation. However, glacier ice is not a closed system and crevasses and lateral water access provides O_2-rich water for further sulfide oxidation and Fe^{3+} reduction is not needed to explain the most sulphate-rich water of the Zermatt area, which contains about 130 mg L^{-1} SO_4^{2-}. In addition, iron is predominantly present in its reduced form in the primary minerals of all rocks of the Zermatt area.

The total amount of solutes carried away by the Mattervispa and by the water removed by the hydroelectric systems can be related to the chemical denudation of the entire area. This aspect of solute generation has not been analyzed in the reported project. However, estimates for denudation rates from the Gornerglacier area range from 500 to 1500 meq m^2 $year^{-1}$ (Brown 2002). For the Rhone glacier and the Oberaarglacier catchments in the Swiss Alps, exclusively in granite dominated basement rocks cation fluxes of about 100 and 550 meq m^2 $year^{-1}$ have been derived, respectively (Hosein et al. 2004).

6 Conclusions

The water composition data show a remarkably consistent correlation with the bedrock lithology of the respective catchment areas. This central observation underlines that the water composition is primarily controlled by the reactions of precipitation water with the exposed minerals of the bedrocks.

The composition of 87 samples of surface water from high alpine Zermatt area delicately reflects the richly diverse geology and the different rock inventory of the local catchments. Dissolving primary minerals of the predominantly metamorphic rocks cause the observed increase of total dissolved solids (TDS) from a few mg L^{-1} in precipitation to typically several 10 s of mg L^{-1} (up to 270 mg L^{-1}) in the surface water of the Zermatt area. The amount and proportion of the major solutes acquired by water–rock interaction depends of the rock type dominating the local catchment and the kinetics of the relevant mineral dissolution reactions.

The net transfer of solutes to the surface waters computed from inverse models shows that very few effective bulk reactions dominate the water composition. The presence and modal amount of sulfide minerals primarily controls and limits TDS of the waters by providing sulfuric acid for calcite and silicate dissolution. If calcite is present in the bedrock, dissolution of the mineral neutralizes the acid produced by sulphide weathering and buffers pH to near neutral to weakly alkaline conditions. If calcite is absent, the process produces low-pH waters in gneiss and granite catchments. It is also concluded that natural low-pH waters (pH <6) in a pristine high-altitude environment

have a geogene origin. A pH ~5 corresponds to the pH of rainwater. However, if TDS of the water is significantly higher than that of rainwater a source of H^+ is required. This is because the hydrolysis reactions responsible for the TDS consume H^+ and increase pH (reaction 5). Thus H^+ must be provided by reactions such as reaction (1). These findings confirm the conclusions by Bassett et al. (1992) that natural low-pH sulphate surface water in the alpine Geneva Creek Basin of the southern Rock Mountains acquired its composition by reaction with sulfide (pyrite) and silicate in basement gneiss and granite. Sulfide-free or -poor bedrocks produce water with very low TDS because here hydrolysis depends on dissolved CO_2. Saturation with atmospheric CO_2 efficiently dissolves calcite but not silicates (Brown 2002; Hosein et al. 2004).

Bassett et al. (1992) also found that only minor amounts of the solute inventory where contributed by atmospheric precipitation. Effects of biomass fluctuations on the water composition (Bowser and Jones 2002) cannot be detected with the sample material of this study. However, we expect this to be a minor issue in the high-alpine Zermatt region.

All samples of this study were taken in a precipitation-free period in September mostly between noon and early evening and thus under similar hydrological and meteorological conditions. However, it can be expected that water composition show seasonal and daytime variations (Hosein et al. 2004; Hindshaw et al. 2011). Enhanced silicate weathering can be expected during low discharge periods (during winter, during early morning). This has been shown for the glacial granite catchment of the Damma glacier (Hindshaw et al. 2011). The Zermatt samples represent a wide variety of catchment lithologies but we assume that the general relationships of the granitic Damma glacier data also apply to other silicate rock catchments. If so, it follows from the Damma glacier study that the Zermatt samples represent relatively short residence time, high-discharge water, with the lowest contribution from silicate weathering during temporal discharge variation.

Dissolution of carbonates is also taken forward by reaction with rain and snowmelt saturated with atmospheric CO_2 (Hosein et al. 2004). However, silicate dissolution by carbonic acid is not an efficient process. Consequently, high-TDS CC water contains a high proportion of sulphate in addition to hydrogen carbonate and high-TDS CS water from granite does generally contain little hydrogen carbonate. MC water from carbonate-free serpentinites have a very low TDS, reflecting the generally also low content of weatherable sulfide minerals in the ultramafic rocks.

Generally, it also follows that silicate mineral dissolution can be significant and dominating even in cold waters and after relatively short reaction times. The key to efficient silicate weathering is a high content of primary sulfide minerals that provide sulphuric acid upon weathering.

Acknowledgements We thank Sigrid Hirth-Walther and Isolde Schmidt for laboratory assistance. The second author gratefully acknowledges financial support from the China Scholarship Council. The Rinne Foundation appreciatively supported two years of fieldwork. We are grateful for comments and suggestions made by two anonymous reviewers, which helped to improve the manuscript. Edwin Gnos provided valued editorial handling of the manuscript.

References

Acker, J. G., & Bricker, O. P. (1992). The influence of pH on biotite dissolution and alteration kinetics at low-temperature. *Geochimica et Cosmochimica Acta, 56,* 3073–3092.

Anderson, S. P., Drever, J. I., Frost, C. D., & Holden, P. (2000). Chemical weathering in the foreland of a retreating glacier. *Geochimica et Cosmochimica Acta, 64,* 1173–1189.

Anderson, S. P., Drever, J. I., & Humphrey, N. F. (1997). Chemical weathering in glacial environments. *Geology, 25,* 399–402.

Appelo, C. A. J., & Postma, D. (2007). *Geochemistry, groundwater and pollution* (2nd ed.). Leiden: A.A. Balkema Publishers.

Aquilina, L., Sureau, J. F., & Steinberg, M. (1997). Comparison of surface-, aquifer- and pore-waters from a Mesozoic basin and its underlying Paleozoic basement, southeast France: Chemical evolution of waters and relationships between aquifers. *Chemical Geology, 138,* 185–209.

Atteia, O. (1994). Major and trace-elements in precipitation on western Switzerland. *Atmospheric Environment, 28,* 3617–3624.

Bagshaw, E. A., Tranter, M., Wadham, J. L., Fountain, A. G., Dubnick, A., & Fitzsimons, S. (2016). Processes controlling carbon cycling in Antarctic glacier surface ecosystems. *Geochemical Perspectives Letters, 2,* 44–54.

Bales, R. C., & Morgan, J. J. (1985). Dissolution kinetics of chrysotile at pH 7 to 10. *Geochimica et Cosmochimica Acta, 49,* 2281–2288.

Barnes, I., Lamarche, V. C., & Himmelbe, G. (1967). Geochemical evidence of present-day serpentinization. *Science, 156,* 830–832.

Barnes, I., & O'Neil, J. R. (1969). Relationship between fluids in some Fresh Alpine-type ultramafics and possible modern serpentinization, Western United States. *Geological Society of America Bulletin, 80,* 1947–1960.

Barnes, I., O'Neil, J. R., & Trescases, J. J. (1978). Present day serpentinization in New-Caledonia, Oman and Yugoslavia. *Geochimica et Cosmochimica Acta, 42,* 144–145.

Barnes, I., Sheppard, R. A., Gude, A. J., Rapp, J. B., & O'Neil, J. R. (1972). Metamorphic assemblages and direction of flow of metamorphic fluids in 4 instances of serpentinization. *Contributions to Mineralogy and Petrology, 35,* 263–273.

Barrie, L. A. (1991). Snow formation and processes in the atmosphere that influence its chemical composition. In: Davies T.D., Tranter M., & Jones H.G. (Eds.), Seasonal snowpacks; processes of compositional change. Proceedings of the NATO Advanced Research Workshop on Processes of Chemical Change in Snowpacks, Maratea, Italy, July 1990. *Series G: Ecological Sciences, 28,* pp. 1–20. Springer, Heidelberg, Germany.

Bartier, D., Ledésert, B., Clauer, N., Meunier, A., Liewig, N., Morvan, G., et al. (2008). Hydrothermal alteration of the Soultz-sous-Forêts granite (Hot Fractured Rock geothermal exchanger)

into a tosudite and illite assemblage. *European Journal of Mineralogy, 20,* 131–142.

Bassett, R. L. (1997). Chemical modeling on the bare rock or forested watershed scale. *Hydrological Processes, 11,* 695–717.

Bassett, R. L., Miller, W. R., Mchugh, J., & Catts, J. G. (1992). Simulation of natural acid sulfate weathering in an alpine watershed. *Water Resources Research, 28,* 2197–2209.

Bearth, P. (1953). Geological map 1:25000 Sheet 535 Zermatt. *Geologischer Atlas der Schweiz.* Schweizerische Geologische Kommission.

Bearth, P. (1967). Die Ophiolithe der Zone von Zermatt-Saas Fee. *Beiträge zur geologischen Karte der Schweiz N.F., 132,* 130.

Blum, A., & Lasaga, A. (1988). Role of surface speciation in the low-temperature dissolution of minerals. *Nature, 331,* 431–433.

Blum, A. E., & Stillings, L. L. (1995). Feldspar dissolution kinetics. In A. F. White & S. L. Brantley (Eds.), *Chemical weathering rates of silicate minerals* (Vol. 31, pp. 291–351)., Reviews in mineralogy Chantilly: Mineralogical Society of America.

Bluth, G. J. S., & Kump, L. R. (1994). Lithologic and climatologic controls of river chemistry. *Geochimica et Cosmochimica Acta, 58,* 2341–2359.

Bowser, C. J., & Jones, B. F. (2002). Mineralogic controls on the composition of natural waters dominated by silicate hydrolysis. *American Journal of Science, 302,* 582–662.

Bricker, O. P., Jones, B. F., & Bowser, C. J. (2003). Mass-balance approach to interpreting weathering reactions in watershed systems. In J. I. Drever (Ed.), *Treatise on geochemistry* (Vol. 5, pp. 119–132). Amsterdam: Elsevier.

Brown, G. H. (2002). Glacier meltwater hydrochemistry. *Applied Geochemistry, 17,* 855–883.

Brown, G. H., Sharp, M. J., Tranter, M., Gurnell, A. M., & Nienow, P. W. (1994). Impact of post-mixing chemical-reactions on the major ion chemistry of bulk meltwaters draining the haut glacier darolla, valais, Switzerland. *Hydrological Processes, 8,* 465–480.

Bruni, J., Canepa, M., Chiodini, G., Cioni, R., Cipolli, F., Longinelli, A., et al. (2002). Irreversible water-rock mass transfer accompanying the generation of the neutral, Mg-HCO_3 and high-pH, Ca-OH spring waters of the Genova province, Italy. *Applied Geochemistry, 17,* 455–474.

Bucher, K., Dal Piaz, GV., Oberhänsli, R., Gouffon, Y., Martinotti, G., & Polino, R. (2003). Blatt 1347 Matterhorn. *Geologischer Atlas der Schweiz, 1:25000, Karte 107.*

Bucher, K., Dal Piaz, G.V., Oberhänsli, R., Gouffon, Y., Martinotti, G., & Polino, R. (2004). Blatt 1347 Matterhorn. *Geologischer Atlas der Schweiz, 1:25000, Erläuterungen zur Karte 107,* pp. 73.

Bucher, K., Fazis, Y., De Capitani, C., & Grapes, R. (2005). Blueschists, eclogites, and decompression assemblages of the Zermatt-Saas ophiolite: High-pressure metamorphism of subducted Tethys lithosphere. *American Mineralogist, 90,* 821–835.

Bucher, K., & Grapes, R. (2009). The eclogite-facies Allalin Gabbro of the Zermatt-Saas ophiolite, Western Alps: A record of subduction zone hydration. *Journal of Petrology, 50,* 1405–1442.

Bucher, K., Stober, I., & Müller-Sigmund, H. (2015). Weathering crusts on peridotite. *Contributions to Mineralogy and Petrology, 169*(5), 1–15.

Bucher, K., Zhang, L., & Stober, I. (2009). A hot spring in granite of the Western Tianshan, China. *Applied Geochemistry, 24,* 402–410.

Bühring, B. (2008). *Analyse von Regenwässern in Zermatt/Schweiz*. Bachelor thesis, Institute of Geosciences, Albert-Ludwigs-Universität Freiburg, Germany.

Burch, T. E., Nagy, K. L., & Lasaga, A. C. (1993). Free-energy dependence of albite dissolution kinetics at 80 °C and pH 8.8. *Chemical Geology, 105,* 137–162.

Cadle, S. H. (1991). Dry deposition to snowpacks. In: Davies T.D., Tranter M., & Jones H.G. (Eds.), Seasonal snowpacks; processes of compositional change. Proceedings of the NATO Advanced Research Workshop on Processes of Chemical Change in Snowpacks, Maratea, Italy, July 1990. *Series G: Ecological Sciences, 28,* Springer, Heidelberg, Germany. pp. 21-66.

Cartwright, I., & Barnicoat, A. C. (2002). Petrology, geochronology, and tectonics of shear zones in the Zermatt-Saas and Combin zones of the Western Alps. *Journal of Metamorphic Geology, 20,* 263–281.

Christner, B. C., Priscu, J. C., Achberger, A. M., Barbante, C., Carter, S. P., Christianson, K., et al. (2014). A microbial ecosystem beneath the West Antarctic ice sheet. *Nature, 512,* 310–313.

Cipolli, F., Gambardella, B., Marini, L., Ottonello, G., & Vetuschi Zuccolini, M. (2004). Geochemistry of high-pH waters from serpentinites of the Gruppo di Voltri (Genova, Italy) and reaction path modelling of CO_2 sequestration in serpentinite aquifers. *Applied Geochemistry, 19,* 787–802.

Cleaves, E. T., Fisher, D. W., & Bricker, O. P. (1974). Chemical weathering of serpentinite in Eastern Piedmont of Maryland. *Geological Society of America Bulletin, 85,* 437–444.

Colin, J. L., Renard, D., Lescoat, V., Jaffrezo, J. L., Gros, J. M., & Strauss, B. (1989). Relationship between rain and snow acidity and air-mass trajectory in eastern France. *Atmospheric Environment, 23,* 1487–1498.

De Caritat, P., & Saether, O. M. (1997). Chemical changes attending water cycling though a catchment—An overview. In O. M. Saether & P. De Carritat (Eds.), *Geochemical processes, weathering and groundwater recharge in catchments* (pp. 381–391). Leiden: Balkema Publishers. **(Chapter 13)**.

Drever, J. I. (1994). The effect of land plants on weathering rates of silicate minerals. *Geochimica et Cosmochimica Acta, 58,* 2325–2332.

Drever, J. I. (1997). *The geochemistry of natural waters—Surface and groundwater environments*. New Jersey: Prentice Hall.

Drever, J. I., & Clow, D. W. (1995). Weathering rates in catchments. In A. F. White & S. L. Brantley (Eds.), *Chemical weathering rates of silicate minerals* (Vol. 31, pp. 463–481). Chantilly: Mineralogical Society of America.

Drever, J. I., & Finley, J. B. (1993). Weathering and pedogenesis at the watershed scale: high-elevavtion catchments in silicate terrains. *Chemical Geology, 107,* 289–291.

Drever, J. I., & Hurcomb, D. R. (1986). Neutralization of atmospheric acidity by chemical-weathering in an alpine drainage-basin in the North Cascade Mountains. *Geology, 14,* 221–224.

Drever, J. I., & Zobrist, J. (1992). Chemical-weathering of silicate rocks as a function of elevation in the southern Swiss Alps. *Geochimica et Cosmochimica Acta, 56,* 3209–3216.

Eichler, A., Schwikowski, M., Furger, M., Schotterer, U., & Gäggeler, H. W. (2004). Sources and distribution of trace species in Alpine precipitation inferred from two 60-year ice core paleorecords. *Atmospheric Chemistry and Physics, 4,* 71–108.

Fleer, V. N. (1982). *The dissolution kinetics of anorthite ($CaAl_2Si_2O_8$) and synthetic strontium feldspar ($SrAl_2Si_2O_8$) in aqueous solutions at temperature below 100 °C: applications to the geological disposal of radioactive nuclear wasters*. PhD thesis, Pennsylvania State University, USA.

Ford, D. C., & Williams, P. W. (1989). *Karst geomorphology and hydrology* (p. 576). Chichester: Wiley.

Garrels, R. M. & Mackenzie, F. T. (1967). Origin of the chemical composition of some springs and lakes. In:W. Stumm (Ed.), *Equilibrium concepts in natural water systems* (pp. 222–242), Washington, DC: American Chemical Society. **(Chap. 10)**

Garrels, R. M., & Mackenzie, F. T. (1971). Gregors denudation of continents. *Nature, 231,* 382–383.

Gislason, S. R., Arnorsson, S., & Armannsson, H. (1996). Chemical weathering of basalt in southwest Iceland: Effects of runoff, age of rocks and vegetative/glacial cover. *American Journal of Science, 296,* 837–907.

Gislason, S. R., Oelkers, E. H., Eiriksdottir, E. S., Kardjilov, M. I., Gisladottir, G., Sigfusson, B., et al. (2008). The feedback between climate and weathering. *Mineralogical Magazine, 72,* 317–320.

Gislason, S. R., Oelkers, E. H., Eiriksdottir, E. S., Kardjilov, M. I., Gisladottir, G., Sigfusson, B., et al. (2009). Direct evidence of the feedback between climate and weathering. *Earth and Planetary Science Letters, 277,* 213–222.

Hilberg, S., & Riepler, F. (2016). Interaction of various flow systems in small alpine catchments: conceptual model of the upper Gurk Valley aquifer, Carinthia, Austria. *Hydrogeology Journal, 24,* 1231–1244.

Hiltbrunner, E., Schwikowski, M., & Körner, C. (2005). Inorganic nitrogen storage in alpine snow pack in the Central Alps (Switzerland). *Atmospheric Environment, 39,* 2249–2259.

Hindshaw, R. S., Tipper, E. T., Reynolds, B. C., Lemarchand, E., Wiederhold, J. G., Magnusson, J., et al. (2011). Hydrological control of stream water chemistry in a glacial catchment (Damma Glacier, Switzerland). *Chemical Geology, 285,* 215–230.

Hosein, R., Arn, K., Steinmann, P., Adatte, T., & Follmi, K. B. (2004). Carbonate and silicate weathering in two presently glaciated, crystalline catchments in the Swiss Alps. *Geochimica et Cosmochimica Acta, 68,* 1021–1033.

Hume, L. A., & Rimstidt, J. D. (1992). The biodurability of chrysotile asbestos. *American Mineralogist, 77,* 1125–1128.

Huss, M., Bauder, A., Werder, M., Funk, M., & Hock, R. (2007). Glacier-dammed lake outburst events of Gornersee, Switzerland. *Journal of Glaciology, 53,* 189–200.

Jenk, T. M. (2006). *Ice core based reconstruction of past climate conditions and air pollution in the alps using radiocarbon*. PhD thesis, Department of chemistry and biochemistry, University of Bern, Switzerland.

Kilchmann, S., Waber, H. N., Parriaux, A., & Bensimon, M. (2004). Natural tracers in recent groundwaters from different Alpine aquifers. *Hydrogeology Journal, 12,* 643–661.

Lasaga, A. C. (1984). Chemical-kinetics of water-rock interactions. *Journal of Geophysical Research, 89,* 4009–4025.

Lasaga, A. C., Soler, J. M., Ganor, J., Burch, T. E., & Nagy, K. L. (1994). Chemical-weathering rate laws and global geochemical cycles. *Geochimica et Cosmochimica Acta, 58,* 2361–2386.

Li, X. P., Rahn, M., & Bucher, K. (2004). Serpentinites of the Zermatt-Saas ophiolite complex and their texture evolution. *Journal of Metamorphic Geology, 22,* 159–177.

Li, X. P., Rahn, M., & Bucher, K. (2008). Eclogite facies metarodingites—phase relations in the system SiO_2–Al_2O_3–Fe_2O_3–FeO–MgO–CaO–CO_2–H_2O: an example from the Zermatt-Saas ophiolite. *Journal of Metamorphic Geology, 26,* 347–364.

Lin, F.-C., & Clemency, C. V. (1981). The kinetics of dissolution of muscovite at 25 °C and 1 atm CO_2 partial pressure. *Geochimica et Cosmochimica Acta, 52,* 143–165.

Maisch, M., Paul, F., & Kääb, A. (2004). Glacier parameters and their changes, 1850–2000. *Hydrological Atlas of Switzerland (Plate 3.10)*. Landeshydrologie und Geologie.

Marques, J. M., Carreira, P. M., Carvalho, M. R., Matias, M. J., Goff, F. E., Basto, M. J., et al. (2008). Origins of high pH mineral waters from ultramafic rocks, Central Portugal. *Applied Geochemistry, 23,* 3278–3289.

Meunier, A., & Velde, B. (1982). Phengitization, sericitization and potassium-beidellite in a hydrothermally-altered granite. *Clay Minerals, 17,* 285–299.

Meybeck, M. (1987). Global chemical-weathering of surficial rocks estimated from river dissolved loads. *American Journal of Science, 287,* 401–428.

Michaud, A. B., Skidmore, M. L., Mitchell, A. C., Vick-Majors, T. J., Barbante, C., Turetta, C., et al. (2016). Solute sources and geochemical processes in Subglacial Lake Whillans, West Antarctica. *Geology, 44,* 347–350.

Nagy, K. L., Blum, A. E., & Lasaga, A. C. (1991). Dissolution and precipitation kinetics of kaolinite at 80 °C and pH 3, the dependence on solution saturation state. *American Journal of Science, 291,* 649–686.

Nagy, K. L., & Lasaga, A. C. (1992). Dissolution and precipitation kinetics of gibbsite at 80 °C and pH 3, the dependence on solution saturation state. *Geochimica et Cosmochimica Acta, 56,* 3093–3111.

Neal, C., & Shand, P. (2002). Spring surface water quality of the Cyprus ophiolites. *Hydrology and Earth System Sciences, 6,* 797–817.

Neal, C., & Stanger, G. (1983). Hydrogen generation from mantle source rocks in Oman. *Earth Planetary Science Letters, 66,* 315–320.

O'Brien, A. K., Rice, K. C., Bricker, O. P., Kennedy, M. M., & Anderson, R. T. (1997). Use of geochemical mass balance modelling to evaluate the role of weathering in determining stream chemistry in five mid-atlantic watersheds on different lithologies. *Hydrological Processes, 11,* 719–744.

Oliva, P., Dupre, B., Martin, F., & Viers, J. (2004). The role of trace minerals in chemical weathering in a high-elevation granitic watershed (Estibere, France): Chemical and mineralogical evidence. *Geochimica et Cosmochimica Acta, 68,* 2223–2243.

Oliva, P., Viers, J., & Dupre, B. (2003). Chemical weathering in granitic environments. *Chemical Geology, 202,* 225–256.

Papastamataki, A. (1977). The alkalinity and the chemical composition of springs issuing from peridotites. *Annales Géologiques des Pays Helleniques, 28,* 551–566.

Parkhurst, D. L. (1995). *User's Guide to PHREEQC—A computer programme for the speciation, reaction path, advective transport, and inverse geochemical calculations. U.S. Geological Survey Water Resources Investigation Report, 95-4227*, p. 143.

Parkhurst, D. L., & Appelo, C. A. J. (1999). *User's guide to PHREEQC (version 2)—A computer programme for the speciation, batch-reaction, one-dimensional transport, and inverse geochemical calculations*. U.S. Geological Survey Water Resources Investigation Report, 95-4259, p. 312.

Parkhurst, D. L., Plummer, L. N., & Thorstenson, D. C. (1982). Balance: A computer program for geochemical calculations. *U.S. Geological Survey Water-Resources Investigations, 82–14*.

Pfeifer, H.-R. (1977). A model for fluids in metamorphosed ultramafic rocks. Observations at surface and subsurface conditions (high pH spring waters). *Schweizerische Mineralogische und Petrographische Mitteilungen, 57,* 361–396.

Pfeifer, H.-R., Derron, M.-H., Rey, D., Schlegel, C., Dalla Piazza, R., Dubois, J. D., et al. (2000). Natural trace element input to the soil-water-plant system, examples of background and contaminated situations in Switzerland, Eastern France and Northern Italy. In B. Markert & K. Friese (Eds.), *Trace metals—Their distribution and effects in the environment* (pp. 33–86). Amsterdam: Elsevier.

Plummer, L. N., & Back, W. (1980). Mass balance approach—Application to interpreting the chemical evolution of hydrologic systems. *American Journal of Science, 280*(2), 130–142.

Plummer, L. N., Michel, R. L., Thurman, E. M., & Glynn, P. D. (1991). Environmental tracers for age dating yong ground water. In W. M. Alley (Ed.), *Regional ground-water quality* (pp. 255–288). Toronto: International Thomson Publishing.

Plummer, L. N., Parkhurst, D. L., & Thorstenson, D. C. (1983). Development of reaction models for groundwater systems. *Geochimica et Cosmochimica Acta, 47,* 665–685.

Price, J. R., Heitmann, N., Hull, J., & Szymanski, D. (2008). Long-term average mineral weathering rates from watershed geochemical mass balance methods: Using mineral modal abundances to solve more equations in more unknowns. *Chemical Geology, 254,* 36–51.

Raiswell, R. (1984). Chemical-models of solute acquisition in glacial melt waters. *Journal of Glaciology, 30,* 49–57.

Raiswell, R., Tranter, M., Benning, L. G., Siegert, M., De'ath, R., Huybrechts, P., et al. (2006). Contributions from glacially derived sediment to the global iron (oxyhydr)oxide cycle: Implications for iron delivery to the oceans. *Geochimica et Cosmochimica Acta, 70,* 2765–2780.

Rimstidt, J. D., & Barnes, H. L. (1980). The kinetics of silica-water reactions. *Geochimica et Cosmochimica Acta, 44,* 1683–1699.

Rimstidt, J. D., & Dove, P. M. (1986). Mineral/solution reaction rates in a mixed flow reactor: Wollastonite hydrolysis. *Geochimica et Cosmochimica Acta, 50,* 2509–2516.

Rose, N. M. (1991). Dissolution rates of prehnite, epidote, and albite. *Geochimica et Cosmochimica Acta, 55,* 3273–3286.

Schnoor, J. L. (1990). Kinetics of chemical weathering: a comparison of laboratory and field rates. In W. Stumm (Ed.), *Aquatic Chemical Kinetics* (pp. 475–504). Chichester: Wiley.

Schott, J., Brantley, S., Crerar, D., Guy, C., Borcsik, M., & Willaime, C. (1989). Dissolution kinetics of strained calcite. *Geochimica et Cosmochimica Acta, 53,* 373–382.

Schwarb, M., Daly, C., Frei, C., & Schär, C. (2001a). Mean Seasonal Precipitation throughout the European Alps 1971–1990. *Hydrological Atlas of Switzerland (Plate 2.7).* Landeshydrologie und Geologie.

Schwarb, M., Daly, C., Frei, C., & Schär, C. (2001b). Mean annual precipitation in the European Alps 1971-1990. *Hydrological Atlas of Switzerland (Plate 2.6).* Landeshydrologie und Geologie.

Sequeira Bragam, M. A., Paquet, H., & Begonha, A. (2002). Weathering of granites in a temperate climate (NW Portugal): Granitic saprolites and arenization. *CATENA, 49,* 41–56.

Steck, A., Bigioggero, B., Dal Piaz, V. G., Escher, A., Martinotti, G., & Masson, H. (1999). Carte tectonique des Alpes de Suisse occidentale. *Carte géologique spéciale N°123*. Swiss National Hydrological and Geological Survey.

Stober, I., Richter, A., Brost, E., & Bucher, K. (1999). The Ohlsbach Plume: Natural release of deep saline water from the crystalline basement of the black forest. *Hydrogeology Journal, 7,* 273–283.

Tardy, Y., Bustillo, V., Roquin, C., Mortatti, J., & Victoria, R. (2005). The Amazon. Bio-geochemistry applied to river basin management Part I. Hydro-climatology, hydrograph separation, mass transfer balances, stable isotopes, and modelling. *Applied Geochemistry, 20,* 1746–1829.

Taylor, A. B., & Velbel, M. A. (1991). Geochemical mass balances and weathering rates in forested watersheds in the southern blue ridge. Effects of botanical uptake terms. *Geoderma, 51,* 29–50.

Tranter, M., Brown, G., Raiswell, R., Sharp, M., & Gurnell, A. (1993). A conceptual-model of solute acquisition by alpine glacial meltwaters. *Journal of Glaciology, 39,* 573–581.

Tranter, M., Sharp, M. J., Lamb, H. R., Brown, G. H., Hubbard, B. P., & Willis, I. C. (2002). Geochemical weathering at the bed of Haut Glacier d'Arolla, Switzerland—a new model. *Hydrological Processes, 16,* 959–993.

Velbel, M. A. (1985). Geochemical mass balances and weathering rates in forested watersheds of the southern blue ridge. *American Journal of Science, 285,* 904–930.

Velbel, M. A., & Price, J. R. (2007). Solute geochemical mass-balances and mineral weathering rates in small watersheds: Methodology, recent advances, and future directions. *Applied Geochemistry, 22,* 1682–1700.

Wadham, J. L., Tranter, M., Skidmore, M. L., Hodson, A. J., Priscu, J. C., Lyons, W. B., et al. (2010). Biogeochemical weathering under ice: Size matters. *Global Biogeochemical Cycles, 24,* GB3025. doi:10.1029/2009GB003688.

Weber, S., & Bucher, K. (2015). An eclogite-bearing continental tectonic slice in the Zermatt-Saas high-pressure ophiolites at Trockener Steg (Zermatt, Swiss Western Alps). *Lithos, 232,* 336–359.

White, A. F., & Blum, A. E. (1995). Effects of climate on chemical-weathering in watersheds. *Geochimica et Cosmochimica Acta, 59,* 1729–1747.

White, A. F., & Brantley, S. L. (1995). Chemical weathering rates of silicate minerals: An overview. In A. F. White & S. L. Brantley (Eds.), *Chemical weathering rates of silicate minerals* (Vol. 31, pp. 1–22). Reviews in mineralogy. Chantilly: Mineralogical Society of America.

White, A. F., & Brantley, S. L. (2003). The effect of time on the weathering of silicate minerals: Why do weathering rates differ in the laboratory and field? *Chemical Geology, 202,* 479–506.

White, A. F., Bullen, T. D., Schulz, M. S., Blum, A. E., Huntington, T. G., & Peters, N. E. (2001). Differential rates of feldspar weathering in granitic regoliths. *Geochimica et Cosmochimica Acta, 65,* 847–869.

White, A. F., & Hochella, M. F. (1992). Surface chemistry associated with the cooling and subaerial weathering of recent basalt flows. *Geochimica et Cosmochimica Acta, 56,* 3711–3721.

White, A. F., Schulz, M. S., Lowenstern, J. B., Vivit, D. V., & Bullen, T. D. (2005). The ubiquitous nature of accessory calcite in granitoid rocks: Implications for weathering, solute evolution, and petrogenesis. *Geochimica et Cosmochimica Acta, 69,* 1455–1471.

Wollast, R. (1990). Rate and mechanism of dissolution of carbonates in the system $CaCO_3$–$MgCO_3$. In W. Stumm (Ed.), *Aquatic chemical kinetic* (pp. 431–445). New Jersey: Wiley-Interscience.